Alma Mater Studiorum · Università di Bologna

Dipartimento di Fisica e Astronomia "Augusto Righi"

Corso di Laurea in Fisica

The physical principles of Concentrating Solar Power Plants

Relatore:

Prof. Lorenzo Rinaldi

Presentata da:

Alok Nath

Anno Accademico 2024/2025

ABSTRACT

L'energia solare è una risorsa ampiamente disponibile e, in linea teorica, sufficiente a soddisfare il fabbisogno energetico mondiale. La crescente consapevolezza della scarsa sostenibilità delle risorse fossili ha stimolato la ricerca di una soluzione basata su fonti rinnovabili. Tra le diverse tecnologie disponibili per convertire l'energia solare in energia elettrica, le centrali solari a concentramento (Concentrated Solar Power, CSP) rappresentano una tecnologia promettente.

Queste centrali convertono la radiazione elettromagnetica in calore, successivamente in lavoro meccanico e infine in energia elettrica, senza l'emissione di gas serra e con impatto ambientale notevolmente inferiore rispetto alle convenzionali centrali termoelettriche.

In questa tesi, partendo dall'analisi della radiazione solare, vengono esaminati i principali passaggi della conversione dell'energia solare in questi impianti: dalla cattura della radiazione, attraverso le leggi dell'ottica geometrica, al trasferimento del calore dal ricevitore mediante un fluido termovettore, fino alla conversione in lavoro meccanico tramite un motore termico. Inoltre, vengono discusse le principali applicazioni attuali e, infine, vengono illustrate le prospettive future di questa tecnologia.

Contents

Introduction

In recent decades, the growing awareness of climate change and the depletion of fossil resources have driven the scientific and technological communities toward the pursuit of renewable, sustainable and low-environmental impact energy sources. Among the various available options, solar energy holds a particularly prominent position due to its abundance and its potential to be converted into electricity through a wide range of technologies.

Concentrating Solar Power plants (CSP), also known as solar thermal power plants, represent one of the main methods for harnessing solar energy. Unlike photovoltaic systems, which directly convert solar radiation into electricity through the photovoltaic effect [1], CSP plants employ mirrors or lenses to concentrate sunlight onto a focal point or along a focal line, thereby generating high-temperature heat. This thermal energy is subsequently used to produce steam that drives turbines connected to electric generators, in a close analogy with conventional thermoelectric power plants. A distinctive advantage of this technology lies in its ability to integrate thermal energy storage systems, which store energy in the form of heat and release it when needed, during the absence of solar radiation. This enables CSP plants to ensure a more continuous and programmable electricity output, effectively overcoming one of the main limitations of non-dispatchable renewable energy sources.

The present work focuses on the physical principles and thermodynamic mechanisms that underlie this class of power plants, and on how these principles are implemented in modern large-scale applications.

The first chapter provides an overview of solar energy and CSP technology, followed by the analysis of the Direct Normal Irradiance (DNI) and how it can be captured minimizing the angle losses through proper solar tracking. This includes the definition of the incident angle, the optical properties, the concentration ratio, and the evaluation of the optical efficiency.

The second chapter covers the thermal performance of the receiver and the Heat Transfer Fluid (HTF), discussing its main physical properties and the equations governing heat transfer through the receiver tubes. Subsequently,

the chapter presents the main thermodynamic cycles used to convert heat into mechanical work followed by the assessment of the overall efficiency of converting DNI to electrical energy.

The third chapter discusses the relevance of CSP technology within the broader context of the global energy transition. It reviews the most deployed CSP configurations (parabolic trough collectors, solar power towers) and presents modern examples of major CSP facilities, and outlines possible future developments of less mature CSP technologies highlighting their respective advantages and disadvantages.

CHAPTER 1

CONCENTRATING SOLAR POWER

1 Electricity production

Electricity can be generated from different primary energy sources by using a variety of energy conversion technologies. Therefore, there are different competing technologies in the electricity market [2], and technologies with lower costs are most preferred from an affordability standpoint. At present, most of the electricity is globally generated by thermal power plants, and these plants are predominantly driven by fossil fuels (coal, oil, and natural gas), as shown in Figure 1.1. Even though at the current stage fossil-fuel-based electricity remains cheaper, the inevitability that fossil fuel will eventually be replaced by solar energy is simply a geological fact: the total recoverable reserve of fossil fuels is finite. In contrast, renewable energy has low intensity of carbon emissions and replenishes itself by natural mechanisms. Furthermore, solar energy directly powers photovoltaic and solar thermal technologies, while indirectly influencing other renewable resources such as wind, hydropower, and biomass [1].

1.1 Solar Energy

Solar energy represents one of the most abundant and widely distributed energy resources on our planet. The Sun emits radiation[1] as a blackbody[2] at an

[1]Radiative heat transfer is the process by which energy is emitted, transmitted, or absorbed in the form of electromagnetic waves. Unlike conduction or convection, radiation does not require a material medium and can occur across a vacuum. The intensity and spectrum of emitted radiation depend on the temperature and emissivity of the surface, as described by the Stefan–Boltzmann law.

[2]A blackbody is an idealized physical object that absorbs all incident electromagnetic radiation, and re-emits energy with a characteristic continuous spectrum that depends only on its absolute temperature.

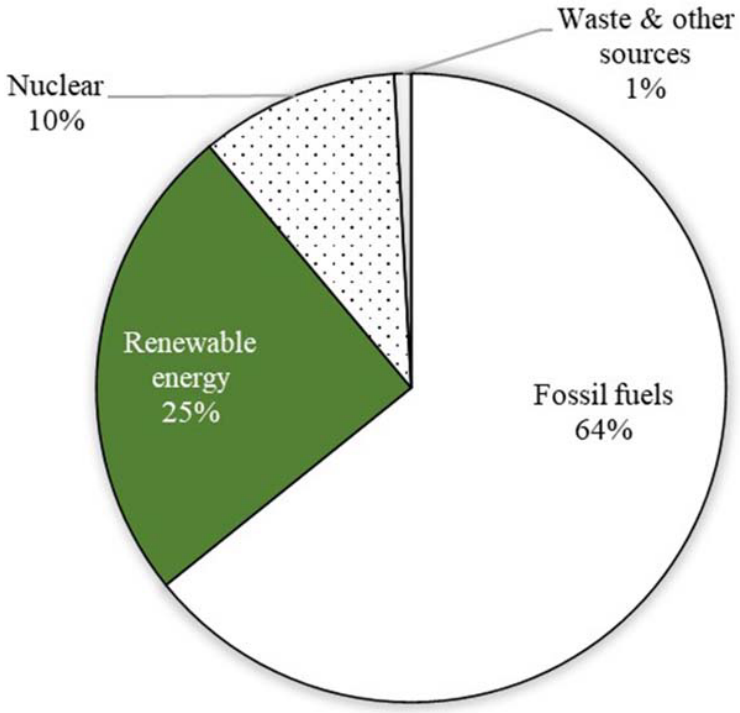

Figure 1.1: Global production of electricity by different primary source of fuel [3].

average temperature of approximately 6000 K [4]. Figure 1.2 shows the solar spectrum. The average power density of solar radiation measured with satellites just outside the Earth's atmosphere is 1366 W/m^2, known as the solar constant [1]. This can be demonstrated empirically considering the sun as a blackbody at a temperature T_{sun} of 5780 K according to the Stefan–Boltzmann law[3]:

$$I_{\text{sun}} = \sigma T_{\text{sun}}^4 \tag{1.1}$$

where I_{sun} is the power emitted per unit area by the Sun. Next by multiplying I_{sun} by the Sun's total surface area ($4\pi R_{\text{sun}}^2$), where R_{sun} is the Sun's radius ($\approx 6.96 \times 10^8$ m), the total luminosity (total power output) of the Sun can be obtained (L_{sun}):

$$L_{\text{sun}} = I_{\text{sun}} \times 4\pi R_{\text{sun}}^2 \tag{1.2}$$

[3]The Stefan–Boltzmann law expresses the total radiant energy flux (irradiance) emitted per unit surface area of a body as $I = \varepsilon\sigma T^4$, where ε is the emissivity (how much the object aproximates a blackbody), $\sigma = 5.670374419 \times 10^{-8}\,\text{W}\,\text{m}^{-2}\,\text{K}^{-4}$ is the Stefan–Boltzmann constant, and T is the absolute temperature. For the Sun, which behaves approximately as a blackbody, $\varepsilon \approx 1$.

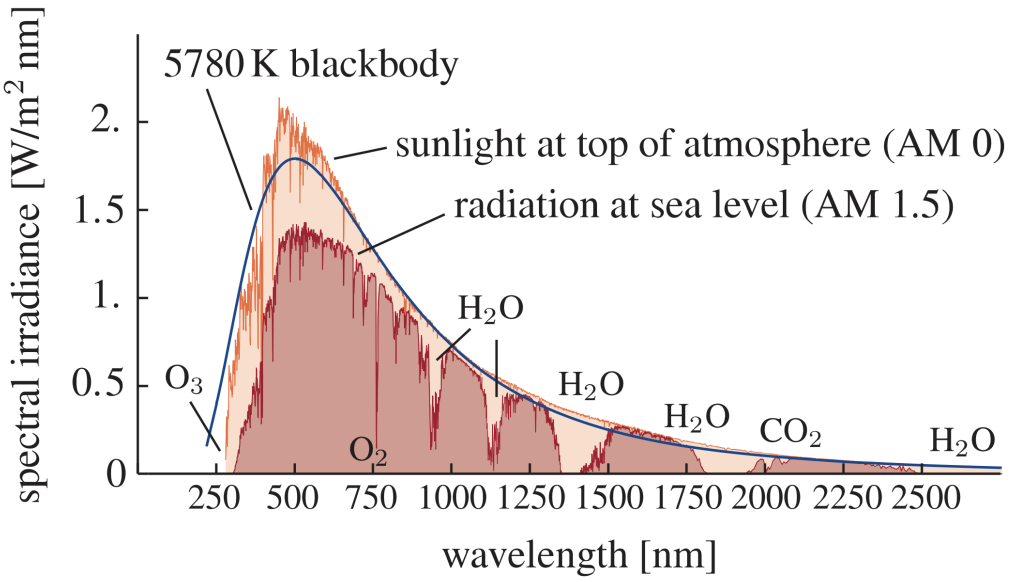

Figure 1.2: Spectrum of solar radiation received outside the atmosphere (AM 0) and compared at sea level (AM 1.5). The elements responsible for the absorption of specific solar wave frequencies are indicated [5].

The total luminosity spreads out over a large sphere with a radius equal to the average Earth-Sun distance D (1 AU, or $\approx 1.496 \times 10^{11}$ m).

$$S = \frac{L_{\text{sun}}}{4\pi D^2} \tag{1.3}$$

This is the solar constant. The calculation yields a value 1361 W/m^2 close to the measured average value of 1366 W/m^2. Finally we can estimate, using the solar constant, the average solar energy that reaches the Earth (using a cross-sectional area of $A = \pi r^2$ with a radius r of 6,371 km) in a year:

$$\text{Annual Solar Energy} = S \times A \times \text{Seconds per Year} \approx 5.46 \times 10^{24} \text{ J} \tag{1.4}$$

Of this immense energy, only a small fraction actually reaches the Earth's surface because of various attenuation effects, which is nevertheless sufficient to largely exceed the current global energy demand (Figure 1.3). The solar radiation that reaches the Earth's surface consists of two components: a direct component (direct solar radiation), also called beam radiation, which arrives without deviation, and a diffuse component, resulting from the scattering of sunlight by molecules and particles in the atmosphere. The sum of these two

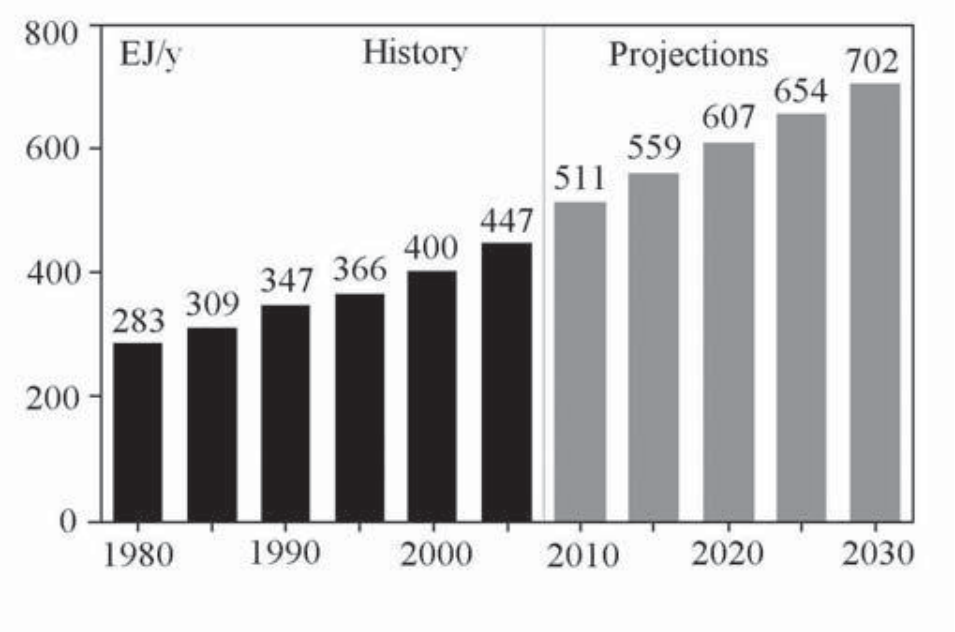

Figure 1.3: World energy consumption divided in historical and projected values [6].

components constitutes the global radiation, a fundamental parameter for assessing the solar potential of a specific site.

Due to atmospheric absorption and scattering, the effective solar radiation at ground level varies depending on several factors such as latitude, altitude, time of day, weather conditions, and season.

To evaluate the solar energy availability of a given location, the concepts of direct normal irradiance (DNI) and annual solar energy per unit area (expressed in $kWh/m^2 \cdot year$) must be introduced. Regions characterized by high insolation (such as desert areas and Mediterranean zones) offer the most favorable conditions for the installation of concentrating solar power (CSP) plants.

In particular, an average annual solar energy value exceeding 2000 kWh/m^2 is generally considered optimal for the deployment of CSP systems. Figure 1.4 shows the annual DNI in the world. To maximize solar capture, CSP power plants often employ solar tracking systems, which continuously align the optical device with the Sun's rays. Therefore, a precise understanding of the characteristics of solar radiation and its spatiotemporal variations represents the starting point for the design and optimization of a solar thermal power plant. Such knowledge enables the proper sizing of collectors, storage systems,

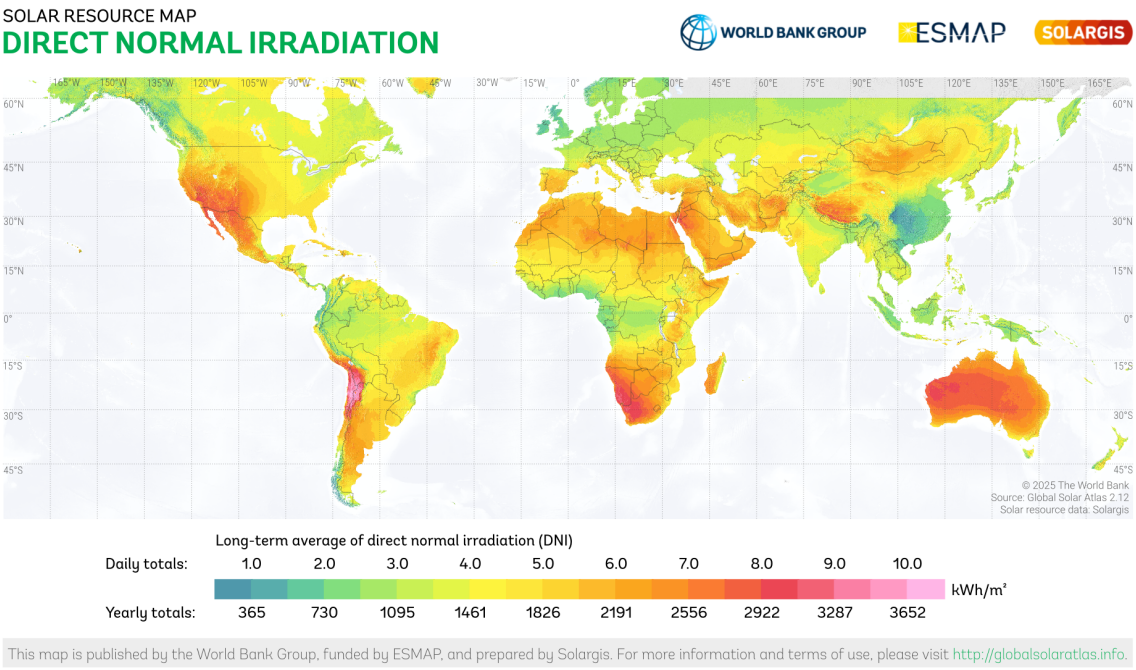

Figure 1.4: Distribution of direct normal irradiation worldwide, with an estimation of daily and yearly DNI [7].

and the thermodynamic cycle, thereby maximizing the overall efficiency of the system.

1.2 Fundamental principles of CSP

Concentrating Solar Power (CSP) technologies convert solar energy into electricity through a thermally driven process based on optical concentration and high–temperature heat conversion. Their operation begins with the collection of direct normal irradiance (DNI), which is reflected by mirrors or lenses and concentrated onto a smaller receiver area, thereby increasing the local solar flux. The concentrated radiation is then absorbed by a heat transfer fluid (HTF), generally synthetic oils and molten salts, whose temperature may rise to values between 300°C and 600°C depending on the specific CSP configuration. The thermal energy stored in the hot HTF is subsequently delivered to a power block, where it generates mechanical work through a thermodynamic cycle, most commonly the Rankine cycle. Mechanical work produced by the turbine is then directly converted into alternating electricity using a generator, ready to be connected to the local power grid. CSP plants natu-

rally incorporate thermal energy storage by holding heat absorbing materials, typically molten salts, in dedicated hot and cold tanks, allowing electricity production to continue even during periods without sunlight. This combination of optical concentration, high-temperature heat transfer, and dispatchable thermodynamic conversion defines the fundamental working principle of CSP technologies and motivates their deployment in regions with high DNI.

1.3 Direct Normal Irradiance

Diffused radiation is the part of the sun radiation that has been scattered and diffused in the Earth's atmosphere and cannot be effectively concentrated by mirrors. So CSP power plants mainly rely on the direct radiation that travels directly from the sun's disc to a receiver surface, whose rays can be traced from the sun's position and used in the computation of solar angles. The Direct Normal Irradiance (DNI,G_{dn}) is a good parameter that indicates the suitability for the deployment of CSP technologies and it can be calculated by the relation [8]:

$$G_{dn} = \frac{G_{gh} - G_{dh}}{\cos\theta_z} \tag{1.5}$$

where G_{gh} is the global irradiance, G_{dh} is the diffused irradiance, whose values can be measured experimentally on a horizontal surface and θ_z is the solar zenith angle (the angle between the sun and the vertical, in detail in chapter 1.4).

1.3.1 Solar Tracking

Solar tracking plays a crucial role in minimizing angular losses of incoming solar radiation on the collector surface. To determine the orientation of the solar beam relative to a given location, several geometric parameters must be defined prior to the computation of the incidence angle [9].

- **The solar declination angle** δ (the angle between the line connecting the Earth's center to the Sun and the Earth's equatorial plane) for any given day of the year can be approximated by the following empirical

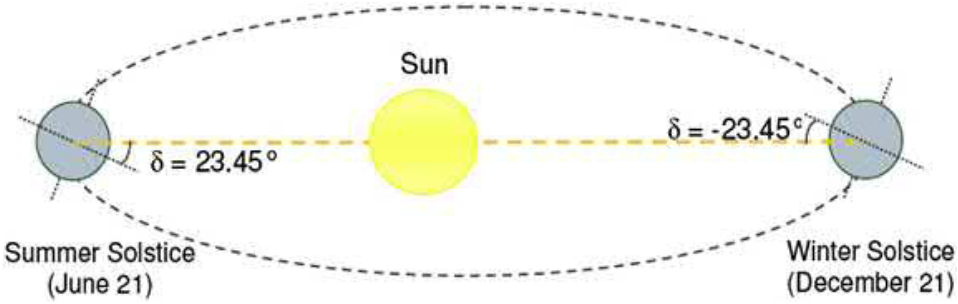

Figure 1.5: Variation of declination angle during a year, depending on the position of the Earth with respect to the Sun [10].

relation:

$$\delta = 23.45^\circ \times \sin\left(\frac{360^\circ}{365} \times (284 + n)\right) \tag{1.6}$$

where n is the day of the year (1 for Jan 1, 365 for Dec 31). Figure 1.5 gives a visual representation of the change during a year.

- **The apparent solar time** (AST) is the time indicated by the Sun's actual position where solar noon occurs when the Sun crosses the local meridian. The length of an apparent solar day changes throughout the year because of the variation of Earth's elliptical orbit and axial tilt.
  The apparent solar time can be related to the local standard time (LST) through the correction of both the equation of time and the difference in longitude as:

$$AST = LST + ET - 4(SL - LL) \tag{1.7}$$

  where LST is the local standard time (in minutes), ET is the equation of time correction (in minutes), SL is the standard meridian longitude of the time zone, and LL is the local longitude (positive eastward, negative westward). The term ET accounts for the non-uniform motion of the Earth in its orbit and axial tilt, and can be approximated as [11]: $ET = 9.87\sin(2B) - 7.53\cos(B) - 1.5\sin(B)$ in which B = 360°(n - 81)/364 and n is the date serial number.

- **The solar hour angle** w represents the angular displacement of the

Sun east or west of the local meridian, corresponding to the Earth's rotation. It is zero at solar noon, negative in the morning, and positive in the afternoon, with a change rate of 15° per hour:

$$w = 0.25^\circ(AST - 720) \tag{1.8}$$

- **The solar zenith angle** θ_z is the angle between the vertical direction and the line joining a given point on the Earth's surface to the center of the Sun, expressed as:

$$\cos(\theta_z) = \sin(\phi)\sin(\delta) + \cos(\phi)\cos(\delta)\cos(w) \tag{1.9}$$

here ϕ is the latitude of the location, w is the solar hour angle, δ is the solar declination angle.

- **The solar altitude angle** a_s is the elevation of the Sun above the horizon, and it is the complement of the zenith angle:

$$a_s = 90^\circ - \theta_z \tag{1.10}$$

- **The solar azimuth angle** γ_s defines the deviation of the Sun's projection on the horizontal plane from the geographic south direction. It can be evaluated by:

$$\gamma_s = \arccos\left(\frac{\sin\delta\cos\phi - \cos\delta\cos w\sin\phi}{\cos a_s}\right) - 180^\circ \tag{1.11}$$

and adjusted according to:

$$\gamma_s = -\gamma_s, \quad \text{if } \sin w > 0 \tag{1.12}$$

where all the variables are the same as previously defined.

To visualize, Figure 1.6 indicates the geometrical relationship of the solar zenith, altitude, and azimuth angles mentioned above.

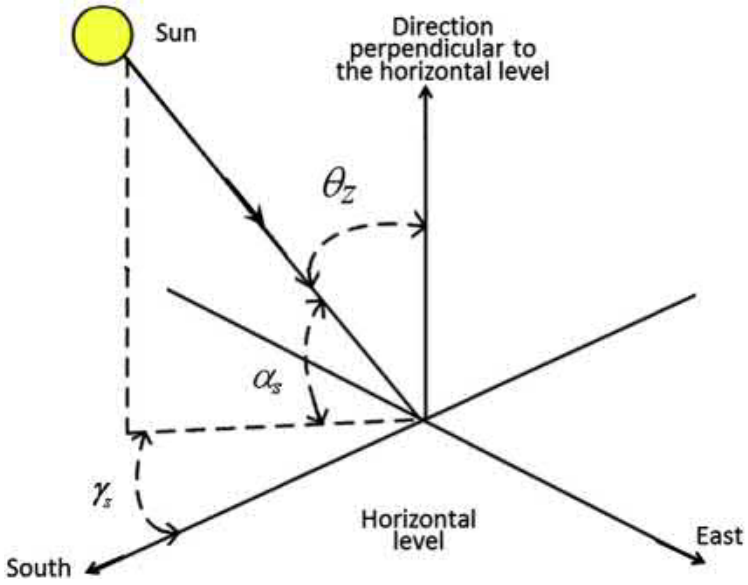

Figure 1.6: Schematic visualization of solar zenith, altitude, and azimuth angles [10].

- **Light-receiving surface slope** β is the angle of the sloped light-receiving surface against the horizontal surface, $0° \leq \beta \leq 180°$, where $\beta > 90°$ refers to the surface facing downward.

Finally, the **the incidence angle** θ represents the angle between the solar beam and the normal to the collector surface, and can be expressed as:

$$\cos\theta = \cos\theta_z \cos\beta + \sin\theta_z \sin\beta \cos(\gamma_s - \gamma) \tag{1.13}$$

where γ denotes the azimuth angle of the collector's normal with respect to the south direction, and the rest of the variables are the same as previously defined. A surface oriented toward the west of south is assigned a positive azimuth angle.

1.4 Optical principles for lenses

The efficiency of a CSP solar system depends on the rigorous application of the optical geometry laws. The primary goal is to maximize the solar energy that is incident on the aperture of the system (a mirror) and direct it to a receiver minimizing energy losses.

1.4.1 Specular Reflection

The operating principle of all parabolic mirrors and heliostats is the law of specular reflection. This law states that the angle of incidence (θ_i) of a light ray on a reflective surface is equal to the angle of reflection (θ_r) relative to the normal (the line perpendicular to the surface at the point of incidence), as expressed mathematically:

$$\theta_i = \theta_r$$

In CSP systems, surfaces are designed with precise geometries (parabolas, dishes, planes) to ensure that parallel solar rays, originating from the solar source, converge at a single focal point or along a specific focal line [11].

1.4.2 Concentration Ratio and Aperture

Two key geometric parameters define the concentration capability of a light converging optical system:

1. **Aperture Area (A_{aperture}):** The effective area of the collector that intercepts the Direct Normal Irradiance (DNI).

2. **Receiver Area (A_{receiver}):** The area of the surface that absorbs the concentrated energy.

The **Geometric Concentration Ratio (C_R)** is defined as the ratio between these two areas [12]:

$$C_R = \frac{A_{\text{aperture}}}{A_{\text{receiver}}}$$

The achievable concentration ratio in a solar concentrator depends on its geometric dimensionality. A **two-dimensional (linear)** concentrator, such as a parabolic trough, focuses incident solar radiation onto a line, whereas a **three-dimensional (point-focus)** system, such as a parabolic dish, concentrates radiation onto a single point. A high C_R is crucial for achieving the high temperatures required by thermodynamic cycles, as higher temperatures lead to greater energy conversion efficiency (Chapter 2, as discussed by the Carnot limit). An upper limit for the concentration ratio, which can be derived from

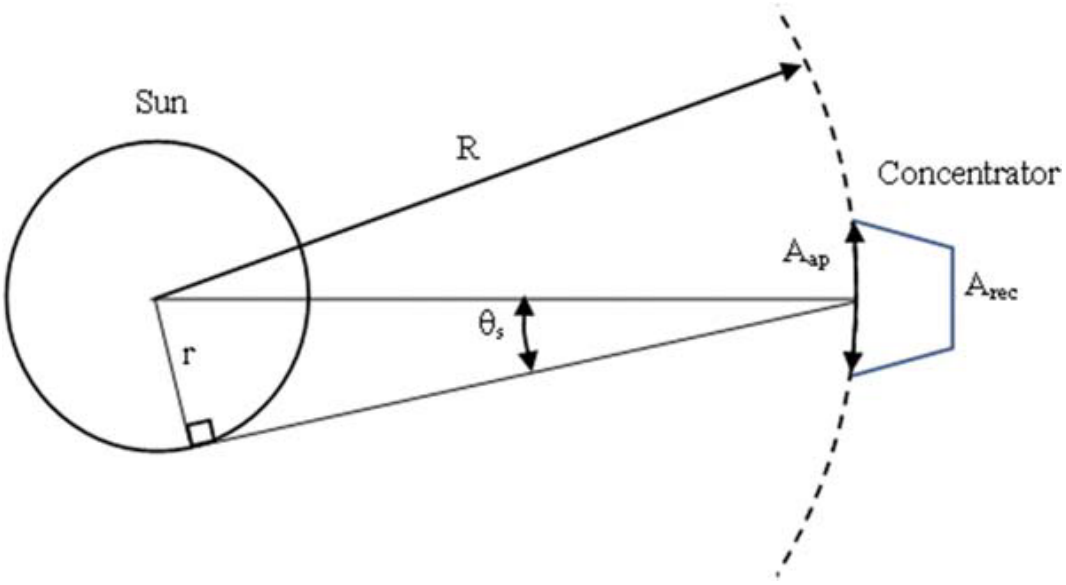

Figure 1.7: Representation of the sun at a temperature T_s and distance R from a concentrator with aperture area A_{ap} and receiver area A_{rec}. The sun radius is r but r_s will be used for clarity [13].

the *second law of thermodynamics*[4] can be obtained [13].

This is equivalent to stating that *etendue* is conserved, which is the measure of the "geometrical extent" of a light beam: *etendue* (G) is proportional to the area of the beam multiplied by the solid angle (the range of angles) the light covers [14]. Considering a circular concentrator of aperture area A_{ap} that intercepts radiation emitted by the Sun, idealized again as a blackbody of radius r_s, temperature T_s, and located at distance R from Earth. The Sun subtends a half-angle θ_s on the concentrator surface, as illustrated schematically in Figure 1.7.

The solid angle in 3D (point-focus, circular) systems is

$$\Omega \approx \pi \sin^2 \theta_s = \pi \frac{r_s^2}{R^2}$$

for a small angle θ, the factor π cancels out in subsequent expressions. In 2D (linear focus) systems, the angular extent is defined using $2 \sin \theta_s$. Assuming a

[4]The second law of thermodynamics states that heat cannot spontaneously flow from a colder body to a hotter one. Applied to radiative exchange, this implies that the entropy of the combined Sun–receiver system must not decrease. Consequently, there exists a finite upper limit to the concentration of solar radiation that can be achieved by any passive optical system (the temperature of the receiver cannot exceed the temperature of the Sun).

perfect concentrator[5], the radiative power intercepted by the aperture can be expressed as:

$$Q_{s\to\mathrm{rec}} = A_{\mathrm{ap}}\,\sigma T_s^4 \left(\frac{r_s^2}{R^2}\right) \tag{1.14}$$

where σ is the Stefan–Boltzmann constant. Similarly, the receiver, considered an ideal blackbody at temperature T_{rec}, radiates (with a maximum angle of $(\sin(90^\circ) = 1)$):

$$Q_{\mathrm{rec}\to s} = A_{\mathrm{rec}}\,\sigma T_{\mathrm{rec}}^4\,E_{\text{rec-s}} \tag{1.15}$$

where $E_{\text{rec-s}}$ represents the fraction of emitted radiation that reaches the Sun. At thermodynamic equilibrium ($T_{\mathrm{rec}} = T_s$), the net heat exchange must vanish:

$$Q_{s\to\mathrm{rec}} = Q_{\mathrm{rec}\to s}. \tag{1.16}$$

Combining Eqs.(1.14) and (1.15) gives:

$$\frac{A_{\mathrm{ap}}}{A_{\mathrm{rec}}} = \frac{r_s^2}{R^2}\,E_{\text{rec-s}}. \tag{1.17}$$

Since the maximum possible value of $E_{\text{rec-s}}$ is unity, the theoretical upper limit of the geometric concentration ratio for an ideal circular concentrator becomes:

$$\left(\frac{A_{\mathrm{ap}}}{A_{\mathrm{rec}}}\right)_{\text{circular,max}} = \frac{r_s^2}{R^2} = \frac{1}{\sin^2\theta_s}. \tag{1.18}$$

For a linear concentrator, the corresponding expression is:

$$\left(\frac{A_{\mathrm{ap}}}{A_{\mathrm{rec}}}\right)_{\text{linear,max}} = \frac{1}{\sin\theta_s}. \tag{1.19}$$

[5]A perfect concentrator is an ideal optical system that reflects or refracts all intercepted rays onto the receiver without losses or aberrations, achieving the maximum thermodynamic limit of concentration.

Given that the Sun subtends an apparent angle of approximately $2\theta_s = 0.53°$, the theoretical limits are:

$$\left(\frac{A_{\text{ap}}}{A_{\text{rec}}}\right)_{\text{circular,max}} \approx 4.5 \times 10^4, \tag{1.20}$$

$$\left(\frac{A_{\text{ap}}}{A_{\text{rec}}}\right)_{\text{linear,max}} \approx 2.1 \times 10^2. \tag{1.21}$$

1.4.3 Optical Efficiency

The optical performance of a concentrating solar collector depends primarily on the **geometry** and **surface properties** of both the concentrator and the receiver. Despite the variety of collector designs, their behavior can be described by a general optical model.

The intensity of solar radiation absorbed per unit area of the receiver, G_{ab}, can be expressed as [11]:

$$G_{ab} = G_{ap}(\rho\alpha\tau\gamma)_n K_{\alpha\tau\gamma} \tag{1.22}$$

where G_{ap} is the effective solar irradiance on the aperture plane, ρ is the **specular reflectance** of the concentrator surface, α is the **absorptance** of the receiver, τ is the **transmittance** of the cover glass (if present), γ is the **intercept factor** representing the fraction of reflected radiation reaching the receiver, and $K_{\alpha\tau\gamma}$ is the **incidence angle modifier** accounting for directional effects. Since the parameters α, τ, and γ vary with the **angle of incidence**, their exact determination may require empirical calibration. The **optical efficiency** of the system, defined as the ratio between absorbed and incident energy fluxes, is given by:

$$\eta_{\text{opt}} = \frac{G_{ab}}{G_{ap}} = (\rho\alpha\tau\gamma)_n K_{\alpha\tau\gamma} \tag{1.23}$$

This formulation shows that the optical efficiency depends jointly on the optical characteristics of both the concentrator and the receiver. Understanding and minimizing these optical losses are fundamental in the design phase of any

CSP plant, as they define the starting point for the analysis of the system's overall energy balance.

In summary, CSP systems rely on the precise understanding of solar radiation, its geometrical concentration, and the optical laws governing reflection and absorption. The concepts introduced in this chapter (such as the concentration ratio, optical efficiency, and solar tracking) form the theoretical foundation for analyzing the thermodynamic behavior of solar receivers and power cycles discussed in the following chapters.

CHAPTER 2

ANALYSIS OF CYCLES AND FLUIDS

2 CSP general structure

Concentrating Solar Power (CSP) systems operate by converting solar radiation into thermal energy and subsequently transforming that energy into mechanical and electrical energy through thermodynamic cycles. The conversion chain can be divided into three fundamental stages:

1. **Solar Collection:** The optical field (mirrors or lenses) concentrates the Direct Normal Irradiance (DNI) onto a receiver surface, where the radiation is absorbed and converted into heat.

2. **Thermal Storage and Transfer:** The absorbed energy is transferred to a heat transfer fluid (HTF) or stored in a thermal reservoir, typically based on molten salts, allowing energy production when sunlight is unavailable.

3. **Power Conversion:** The stored thermal energy drives a thermodynamic cycle, such as the Rankine cycle, to produce mechanical work and ultimately electricity.

Figure 2.1 shows the general structure of a CSP power plant. In a concentrating solar power (CSP) plant, the power block converts the collected thermal energy into electrical energy. Its main components are a heat engine and an electric generator. The engine extracts heat from the receiver (hot reservoir), converts part of it into mechanical work, and rejects the remainder to a cold sink.

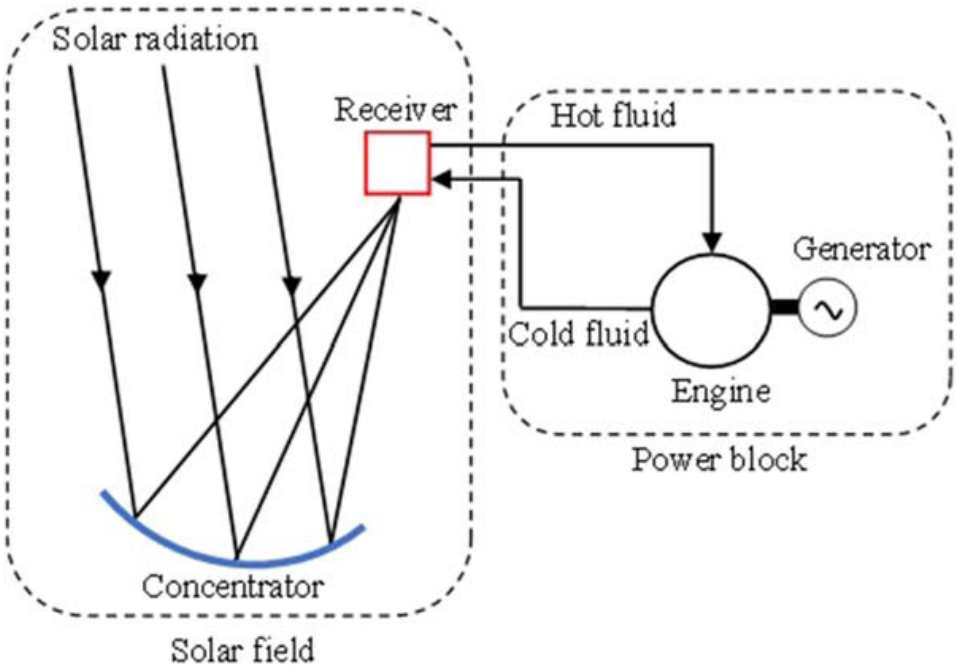

Figure 2.1: Components of a basic concentrating system and the connection between its components in a CSP system [15].

2.1 Thermal Performance of the Receiver

Receivers exhibit significant variations in geometry and operating temperature depending on the type of concentrating system used, therefore they have different heat loss characteristics. Consequently, each design requires specific analysis. Nonetheless, their performance can be described with a general energy balance relation. The useful thermal power extracted from the receiver can be written as [16]:

$$\dot{Q}_u = A_{ap} G_{ab} - \dot{Q}_{loss} \tag{2.1}$$

where A_{ap} is the aperture area, G_{ab} is the absorbed solar radiation per unit area, and $\dot{Q}_{loss}$ represents total thermal losses due to convection, conduction, and radiation. Alternatively, the useful heat can be expressed as the enthalpy[6]

[6]The term $C_{p,htf}(T_{htf,out} - T_{htf,in})$ represents the change in specific enthalpy (Δh_{htf}) of the heat transfer fluid between the inlet and outlet states. For a process occurring at constant pressure, the change in enthalpy is equal to the heat transferred to the system (per unit mass). The equation $Q_u = \dot{m}_{htf} \Delta h_{htf}$ is the fundamental statement of the first law of thermodynamics for a steady-flow process.

increase of the heat transfer fluid (HTF):

$$\dot{Q}_u = \dot{m}_{htf} C_{p,htf} (T_{htf,out} - T_{htf,in}) \tag{2.2}$$

where $\dot{m}_{htf}$ is the mass flow rate, $C_{p,htf}$ the specific heat capacity of the HTF at constant pressure, and $T_{htf,in}$ and $T_{htf,out}$ are the inlet and outlet temperatures, respectively. The receiver thermal efficiency is then defined as:

$$\eta_{rec} = \frac{\dot{Q}_u}{A_{ap} G_{ab}} \tag{2.3}$$

A higher value of η_{rec} indicates a more effective transfer of solar energy from the receiver surface to the heat transfer fluid, which is crucial for improving the overall thermodynamic efficiency of the plant.

2.2 Heat Transfer Mechanisms

Heat transfer represents the flow of thermal energy driven by a temperature gradient, occurring through three fundamental modes: conduction, convection, and radiation. In the receiver, heat generated from absorbed solar radiation is transported to the heat transfer fluid (HTF) primarily through conduction and convection, while radiation plays a secondary role in the internal energy exchange process.

Heat conduction[7] occurs through the absorber wall, transmitting heat from the external surface exposed to concentrated solar radiation toward the internal surface in contact with the HTF. Subsequently, the energy is transferred to the HTF via convective mechanisms.

The efficiency of this process depends on the thermophysical properties of the

[7] Heat conduction is the transfer of thermal energy within a material due to a temperature gradient, resulting from the microscopic motion and interaction of particles. The rate of heat transfer by conduction is governed by Fourier's law, which states that the heat flux $\mathbf{q}$ is proportional to the negative of the temperature gradient, expressed as:

$$\mathbf{q} = -k \nabla T$$

where k is the thermal conductivity of the material ($\mathrm{W/m \cdot K}$) and ∇T is the temperature gradient. This implies that heat flows from regions of higher temperature to regions of lower temperature.

HTF [17], such as thermal conductivity, specific heat capacity, and viscosity, as well as operational parameters like mass flow rate and inlet/outlet temperatures. These factors determine the rate of heat exchange and, consequently, the overall thermal efficiency of the receiver.
Convection, which may occur in either laminar or turbulent regimes depending on the flow conditions, will be examined in the following sections.
Another important aspect to keep in mind is the operating temperature of the fluid before it starts degrading.
The selection of an appropriate HTF is thus critical, as it directly influences the temperature attainable at the receiver and the performance of the entire concentrating solar power CSP system.

2.2.1 Heat Transfer Coefficient

The efficiency of heat transfer between the absorber internal wall and the flowing heat transfer fluid (HTF) is a key factor in determining the overall performance. This is characterized by the **convective heat transfer coefficient** (h), which quantifies the rate of heat exchange between the surface and the fluid [18]. The relationship between the convective coefficient, the internal tube diameter (D_i), and the thermal conductivity of the fluid (k) is expressed through the **Nusselt number** (Nu):

$$Nu = \frac{hD_i}{k} \tag{2.4}$$

The Nusselt number is a dimensionless measure of the enhancement of heat transfer through convection relative to pure conduction across the same temperature gradient. It is typically expressed as a function with other dimensionless parameters that describe the flow regime (Re) and thermal transport properties of the fluid (Pr).

Reynolds Number (Re)**:** The Reynolds number determines the nature of the flow (laminar or turbulent) and is given by:

$$Re = \frac{\rho U D_i}{\mu} \tag{2.5}$$

where ρ is the fluid density, U is the average flow velocity, and μ is the dynamic viscosity and D_i is the characteristic length (typically the hydraulic diameter of the tube).

Prandtl Number (Pr)**:** The Prandtl number expresses the ratio of momentum diffusivity to thermal diffusivity:

$$Pr = \frac{\mu C_p}{k} \tag{2.6}$$

where C_p is the specific heat capacity of the fluid at constant pressure. This number provides insight into the relative thickness of the velocity and thermal boundary layers.
These dimensionless groups enable the evaluation of convective heat transfer performance for different heat transfer fluids and flow regimes.

2.2.2 Specific Heat Capacity

The **specific heat capacity** (C_p) is the most important energetic property. It defines the amount of thermal energy a fluid can store per unit mass for a one Kelvin temperature increase. A high C_p (and high density ρ) is desirable because it allows for the transfer of a large amount of heat while minimizing the required mass flow rate ($\dot{m}$), thereby optimizing pump work and pipe sizing according to [11]:

$$Q_{\text{useful}} = \dot{m} \cdot C_p \cdot \Delta T \tag{2.7}$$

where Q_{useful} is the useful heat transfer rate, $\dot{m}$ is the mass flow rate, C_p is the specific heat capacity at constant pressure, and ΔT is the change in temperature.

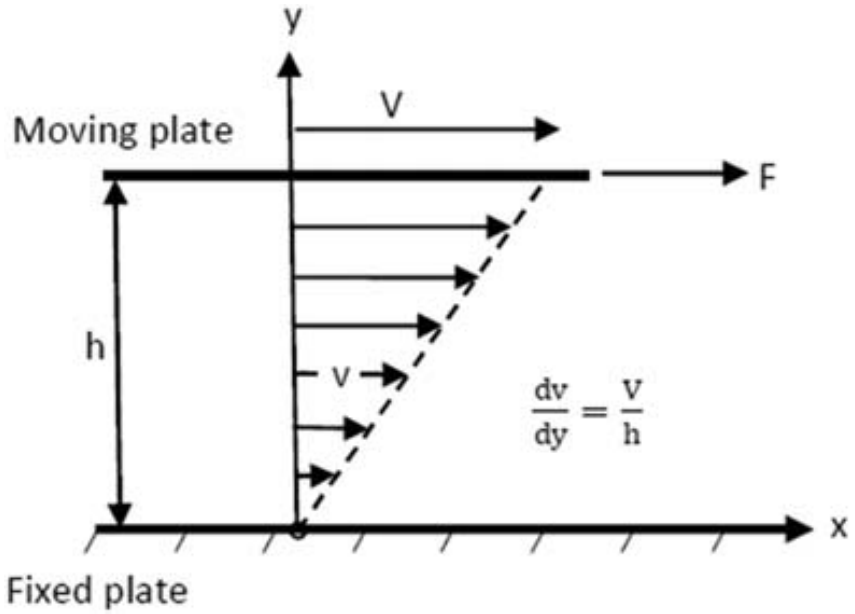

Figure 2.2: Fluid flow between two parallel plates in a newtonian fluid with a simple form of the gradient of the velocity [19].

2.2.3 Viscosity and Flow Regime

Viscosity quantifies a fluid's internal resistance to deformation under shear stress. It arises from intermolecular interactions and momentum exchange between adjacent layers of moving fluid particles, which generate internal friction opposing relative motion [19]. The strength of cohesive and adhesive forces between molecules determines the magnitude of this property, making viscosity a fundamental transport coefficient in fluid mechanics.

A form of viscosity can be introduced, the **dynamic viscosity** (μ). Dynamic viscosity characterizes the proportionality between shear stress and the velocity gradient in a fluid. Depending on the relation between the parameters, a fluid can be Newtonian (if it's a linear relation, shown in Figure 2.2) or non Newtonian.

Mathematically, a **Newtonian fluid** is described by Newton's law of viscosity:

$$\tau = \mu \frac{dV}{dy} \tag{2.8}$$

where τ is the shear stress, μ is the dynamic viscosity, and $\frac{dV}{dy}$ is the velocity gradient perpendicular to the flow direction.

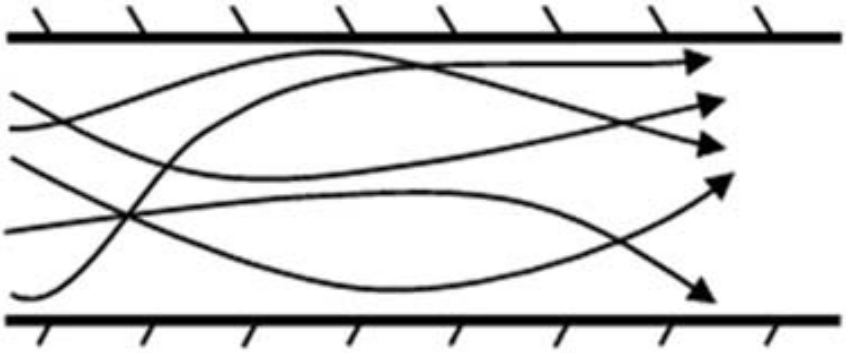

Figure 2.3: Visual example of turbulent flow in a fluid [15].

A **non Newtonian fluid** can be expressed as a general non linear relationship:

$$\tau = K \left(\frac{dV}{dy} \right)^n \tag{2.9}$$

where K is the consistency index, and n is the flow behavior index.
Viscosity is related to the flow regime through the **Reynolds number** (Re) as seen in Eq. (2.5).
The Reynolds number provides a physical measure of whether viscous effects dominate or can be neglected. When $Re > 4000$, the flow is generally **turbulence-dominated**, the viscous dissipation is significant and the flow is more susceptible to turbulence (shown in Figure 2.3). Conversely, when $Re < 2300$, viscous forces prevail, leading to **laminar** and highly ordered motion.

In the context of solar receiver systems, viscosity significantly affects the convective heat transfer coefficient and overall receiver efficiency, since it governs the boundary layer development and flow stability within the absorber tubes.

2.3 Fluid Dynamics

2.3.1 Continuity Equations

To describe the behavior and properties of the HTF in each part of CSP in the flow conduction system, especially during the initial designing part of the complex, the **Navier-Stokes** equations can be used. These are three sets of partial nonlinear differential equations which are derived by the conservation

of mass, momentum and energy, assuming the fluid behaves like a continuum rather than treating it as discrete particles [20].
With prior knowledge of the fluid properties (like the dynamic viscosity, the specific heat capacity, the thermal conductivity and the density of the HTF, with an equation of state for the fluid if it's compressible), the solution of these equation gives the velocity field at each point of the fluid, the pressure distribution throughout the system, the fluid motion (how it accelerates because of general forces and viscous forces), the flow pattern (laminar or turbulent) and how the properties of the fluid vary with temperature.
The knowledge of these variables can be used to improve the overall efficiency of the CSP plant:

- **Velocity**: higher fluid velocity can increase the convective heat transfer and rate of heat absorption in the receiver, but it can also increase the friction and pressure drops.
- **Pressure**: pressure determines the fluid flow (from high to low pressure, so it can require more pump power), as well the thermodynamical efficiency (with the increase of boiling point, so the fluid can reach higher temperature).
- **Temperature**: higher temperature translate to more thermodynamical efficiency, as well as more heat losses from different effects.
- **Density**: density impacts the amount of energy for unit volume the HTF can transport (it is solved for in case the fluid is compressible).
- **Turbulence**: Turbulent flow significantly enhances the mixing and convective heat transfer between the receiver walls and the fluid compared to laminar flow. This allows for faster and more efficient heat absorption. Though this state is preferred, it can also increase dissipation by friction.

From a computational point of view, the Navier-Stokes equations are preferred in the conservation form for its applicability and precision (without the material derivative) [21].

2.3.2 Mass Equation

For a viscous flow (where viscosity effects are present, which is valid almost for all fluids), the law of conservation of mass states that mass cannot be created nor destroyed.

In mathematical form it can be expressed as:

$$\frac{\partial \rho}{\partial t} + \frac{\partial(\rho u)}{\partial x} + \frac{\partial(\rho v)}{\partial y} + \frac{\partial(\rho w)}{\partial z} = 0 \tag{2.10}$$

where ρ is the fluid density, u, v, and w are the velocity components in the x, y, and z directions, respectively.

This equation states that the mass flow entering an infinitesimal control volume must equal the mass flowing out, assuming no accumulation or losses, for example through a leakage.

For incompressible fluids, where the density is constant, Eq. (2.10) reduces to the simplified form:

$$\frac{\partial u}{\partial x} + \frac{\partial v}{\partial y} + \frac{\partial w}{\partial z} = 0 \tag{2.11}$$

The conservative formulation of Eq. (2.10) is generally preferred for numerical and physical modeling of HTFs, as it ensures strict conservation of mass within discretized computational domains and are able to capture sharp changes or discontinuities in the flow field.

2.3.3 Momentum Equation

The law of conservation of momentum states that the rate of change of momentum of a fluid element is equal to the sum of external forces acting on it. For a Newtonian viscous fluid in Cartesian coordinates, the momentum equations in the conservative form can be expressed as:

$$\frac{\partial(\rho \mathbf{V})}{\partial t} + \nabla \cdot (\rho \mathbf{V}\mathbf{V}^T) = -\nabla p + \nabla \cdot \boldsymbol{\tau} + \rho \mathbf{g} \tag{2.12}$$

where $\mathbf{V} = (u, v, w)$ is the velocity vector ($\mathbf{V}^T$ is the transpose), ρ is the density, p is the thermodynamic pressure, $\mathbf{g}$ is the gravitational acceleration, and $\boldsymbol{\tau}$ is

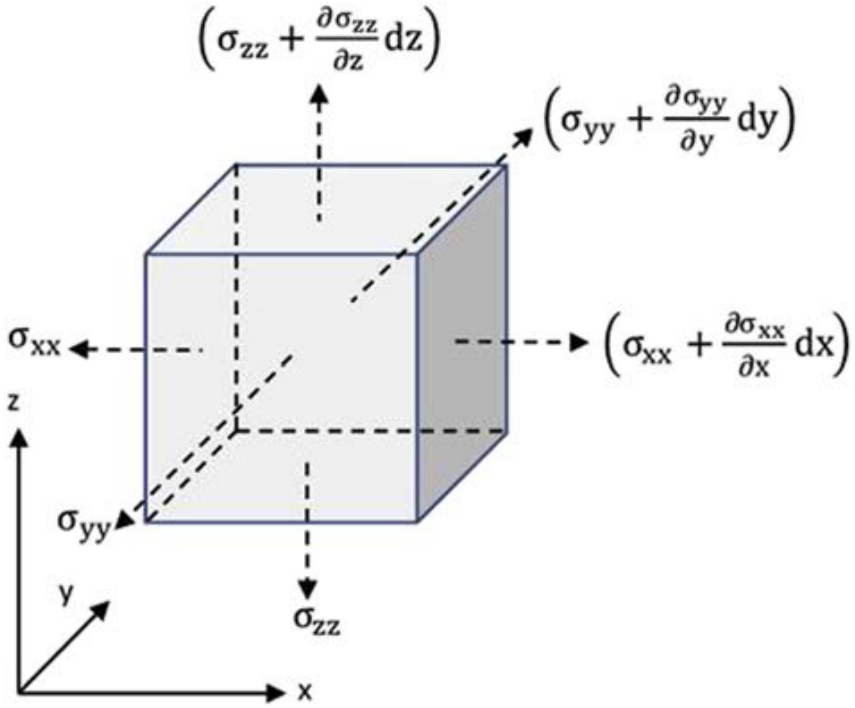

Figure 2.4: Representation of total shear stresses that are acting on a infinitesimal volume of the fluid [15].

the stress tensor, defined for a Newtonian fluid as:

$$\tau_{ij} = \mu \left(\frac{\partial v_i}{\partial x_j} + \frac{\partial v_j}{\partial x_i} \right) - (P_m + \frac{2}{3}\mu(\nabla \cdot \mathbf{V}))\delta_{ij} \tag{2.13}$$

where μ is the dynamic viscosity, δ_{ij} is the Kronecker delta and P_m is the average normal stress: $P_m = \frac{\sigma_{xx}+\sigma_{yy}+\sigma_{zz}}{3}$.
The first two terms of Eq. (2.12) represent respectively the local rate of change of momentum ($\frac{\partial(\rho \mathbf{V})}{\partial t}$) and the convective term of the momentum ($\nabla \cdot (\rho \mathbf{V}\mathbf{V}^T)$). The last term suggests a new definition of the thermodynamical pressure as: $p = P_m + \frac{2}{3}\mu \nabla \cdot \mathbf{V}$ (used in Eq. (2.12)), where the factor $\frac{2}{3}\mu$ is empirically determined and can be replaced by a constant for a general fluid obtained experimentally, also known as Λ bulk viscosity that influences the relative volume rate of change $\nabla \cdot \mathbf{V}$.

The Eq. (2.12) derives from considering the total net internal (given by the stress tensor) and external forces f_{Bx} acting on a face (for example in the x direction) of a infinitesimal cube volume is equal to the variation of the momentum in the volume $\rho \frac{Du}{Dt}$ (as shown in Figure 2.4):

$$\rho \frac{Du}{Dt} = \frac{\partial \tau_{xx}}{\partial x} + \frac{\partial \tau_{yx}}{\partial y} + \frac{\partial \tau_{zx}}{\partial z} + f_{Bx} \tag{2.14}$$

Where the material derivative is expressed as: $\frac{D}{Dt} = \frac{\partial}{\partial t} + (\vec{u} \cdot \nabla)$.
This conservative form of Eq. (2.12) is particularly advantageous in computational fluid dynamics (CFD) and thermal simulations of CSP receivers, since it guarantees the correct accounting of momentum transport through control surfaces.

2.3.4 Energy Equation

The conservation of energy describes the transport and transformation of internal, kinetic, and potential energy within the fluid. For a viscous compressible flow, the energy equation in conservative form reads:

$$\frac{\partial}{\partial t}(\rho E) + \nabla \cdot (\rho \mathbf{V} E) = -\nabla \cdot (p\mathbf{V}) + \nabla \cdot (\boldsymbol{\tau} \mathbf{V}) - \nabla \cdot \mathbf{q} + \rho \mathbf{g} \cdot \mathbf{V} + \dot{q} \tag{2.15}$$

where E is the total energy defined by $E = \left(e + \frac{V^2}{2}\right)$ with e representing the internal energy per unit mass (directly related to the specific heat capacity), $\mathbf{q}$ is the heat flux vector given by Fourier's law $\mathbf{q} = -k\nabla T$ and $\dot{q}$ represents volumetric heat sources such as absorbed solar radiation.
The term $\frac{\partial}{\partial t}(\rho E)$ is the local rate of change of energy per unit volume and $\nabla \cdot (\rho \mathbf{V} E)$ is the convective term of energy per unit volume.
The term $-\nabla \cdot (p\mathbf{V})$ is the work done by pressure forces, the term $\nabla \cdot (\boldsymbol{\tau} \mathbf{V})$ represents viscous dissipation (not negligible in high-temperature fluids such as molten salts or liquid metals), the term $\nabla \cdot \mathbf{q}$ is the rate of heat transfer by conduction while $\rho \mathbf{g} \cdot \mathbf{V}$ represent the rate at which external body forces (per unit mass) do work on the fluid (gravity in this case).
The derivation of Eq. (2.15) is based on the first law of thermodynamics for a moving infinitesimal volume of fluid. It states that rate of change of the energy inside the volume is equal to the net heat flux entering and leaving the volume and the work done on the element due to the forces applied. For the

heat exchange it keeps track of two major processes: volumetric heating (like absorption and radiation emission) and conduction transfer effects.
The conservative form of energy ensures the strict conservation of total energy (including internal and kinetic energy) throughout the computational domain ensuring numerical stability and accuracy when dealing with complex heat transfer mechanisms and potential strong thermal gradients or discontinuities within the fluid flow.

2.3.5 Considerations on the equations

In some cases, under appropriate assumptions, the Navier–Stokes equations can be simplified into forms that are easier to solve analytically. For example, in laminar flow conditions and for a Newtonian fluid, the equations reduce to equations that may admit analytical solutions with well-defined velocity profiles. However, in solar receivers the preferred regime is usually turbulent flow, since turbulence enhances mixing and greatly improves convective heat transfer. In the turbulent regime, the Navier–Stokes equations become extremely difficult to solve because of their intrinsic nonlinearity and the wide range of spatial and temporal scales involved. For this reason only numerical approximations can be obtained using computational solvers.

2.4 Heat Transfer Fluids

In modern CSP plants, the most employed HTFs for application are divided into two categories [22]:

- **Synthetic Oils:** synthetic oils offer good stability up to approximately 400°C. Beyond this temperature, chemical bonds break down (thermal cracking), limiting the maximum achievable efficiency. They offer an advantage during start up of the plant as they have a low freezing point and do not oxidize the plant piping significantly.
- **Molten Salts:** Stable up to 600°C or more, allowing operation at higher temperatures and thus higher efficiencies. They possess a melting point

of around 230°C and require an anti-freezing system. They are known for their corrosive nature.

The choice of HTF is determined by the purpose: when the temperatures reached are not very high (like in parabolic trough), synthetic oils are preferred for their easier startup, while for higher temperatures molten salts are used. The commonly used synthetic oil is Therminol VP-1 (26.5% biphenyl and 73.5% diphenyl oxide) while the molten salt preferred is Solar Salt ($NaNO_3$ 60%, KNO_3 40%) which is also used in thermal energy storage because of its higher heat capacity.

Table 1 reports their properties in function of the temperature.

Therminol VP-1	
Density [kg/m^3]	$1083.25 - 0.90797 \cdot T + 0.00078116 \cdot T^2 - 2.367 \cdot 10^{-6} \cdot T^3$
Dynamic Viscosity [cP]	248
Thermal conductivity [W/(K · m)]	$171.5 \cdot T^{-}1.15$
Heat capacity [kJ/(°C · kg)]	$0.1377 - 8.19 \cdot 10^{-5} \cdot T - 1.922 \cdot 10^{-7} \cdot T^2 + 2.5 \cdot 10^{-11} \cdot T^3$
Solar Salt	
Density [kg/m^3]	$2090 - 0.63 \cdot T$
Dynamic Viscosity [cP]	$71{,}645 \cdot T^{-1.763}$
Thermal conductivity [W/(K · m)]	$0.3804 + 3.452 \cdot 10^{-4} \cdot T$
Heat capacity [kJ/(°C · kg)]	$1.5404 + 3.0924 \cdot 10^{-5} \cdot T$

Table 1: Thermo-physical properties of Therminol VP-1 and Solar Salt depending on temperature T(°C) [22].

All in all, considering the higher cost of syntetic oil is balanced by the fact that molten salt requires higher plant maintenance costs, minor differences are expected ($<\pm 5\%$) in terms of overall power productivity of the CSP plant when the thermal oil is replaced with molten salts. Some other HTF can be used like water in CSP plants that don't achieve high temperatures which, in case of water, is also used as the working fluid in the heat engine (direct configuration).

2.5 Thermodynamics cycles

The fluid dynamic description of the heat transfer fluid provides the velocity, pressure and temperature fields that define how the solar energy is distributed and transported within the receiver. However, the efficiency of a CSP plant depends on how this transported energy is transformed into useful work. For this reason, the thermodynamic behaviour of the HTF at the outlet of the receiver must be linked to the power block. For this purpose, several thermodynamic cycles are presented: some currently used in CSP plants (Rankine cycle) and others less applied or still under study for future applications (Brayton, Stirling, Kalina cycles).

2.5.1 Carnot Cycle

The Second Law of Thermodynamics fundamentally governs the direction and efficiency of energy conversion processes. The Kelvin-Planck formulation states:

"It is impossible to construct a heat engine that, operating in a cycle, produces no effect other than the extraction of heat from a single thermal reservoir and the performance of an equivalent amount of work".

Put in other words, to produce mechanical work there must be a heat flow from a hot reservoir to a cold reservoir. The Carnot cycle defines the theoretical maximum efficiency for any heat engine operating between two thermal reservoirs T_H and T_C, as illustrated in Figure 2.5.

It consists of two reversible isothermal and two isentropic transformations, providing an upper limit for real cycles. Its efficiency is given by:

$$\eta_{car} = \frac{W}{Q_H} = \frac{T_H - T_C}{T_H} \tag{2.16}$$

where W is the useful work, Q_H the transferred heat from the hot reservoir, and $T_H > T_C$. This can be derived by considering the principle of entropy[8] [23]. In

[8]Entropy is a thermodynamic quantity that measures the degree of energy dispersion in a system. For a reversible heat transfer, it is defined as $dS = \frac{\delta Q_{\text{rev}}}{T}$, providing a precise direction of spontaneous processes: entropy tends to increase in irreversible transformations

an ideal reversible cycle (such as the Carnot cycle), the net change in entropy of the universe is zero ($\Delta S_{\text{universe}} = 0$). Heat Q_H is absorbed isothermally at T_H and heat Q_C is rejected isothermally at T_C. The entropy changes are thus:

$$\Delta S_H = \frac{Q_H}{T_H} \quad \text{and} \quad \Delta S_C = -\frac{Q_C}{T_C}$$

Since the cycle is reversible, $\Delta S_H + \Delta S_C = 0$, from which the fundamental relationship follows:

$$\frac{Q_H}{T_H} = \frac{Q_C}{T_C} \quad \text{or} \quad \frac{Q_C}{Q_H} = \frac{T_C}{T_H}$$

The thermal efficiency (η) of any heat engine is defined as the ratio of the net work produced ($W = Q_H - Q_C$) to the heat input (Q_H):

$$\eta = \frac{W}{Q_H} = \frac{Q_H - Q_C}{Q_H} = 1 - \frac{Q_C}{Q_H}$$

Substituting the temperature relationship yields the final expression for the Carnot efficiency (η_{Carnot}) Eq. (2.16).

Although this represents an ideal case, this formula highlights that the efficiency depends exclusively on the ratio between the temperature of the cold source (T_C, the environment) and that of the hot source (T_H, the solar receiver), underscoring the crucial importance of operating at the highest possible temperatures in CSP plants. In solar thermal applications, T_H is constrained by material limits and the achievable receiver temperature, typically below 1000 K.

2.5.2 Rankine Cycle

The Rankine cycle is a practical realization of a vapor power cycle and forms the foundation of modern steam-based CSP plants. A basic real Rankine system comprises a heat source (receiver), a turbine, a condenser, and a feedwater pump and its T-s diagram is shown in Figure 2.6. Water typically serves as the working fluid. Turbines and pumps in this system are classified as turbomachines, which transfer energy between a rotating shaft and a continuously

and remains constant only in ideal reversible ones.

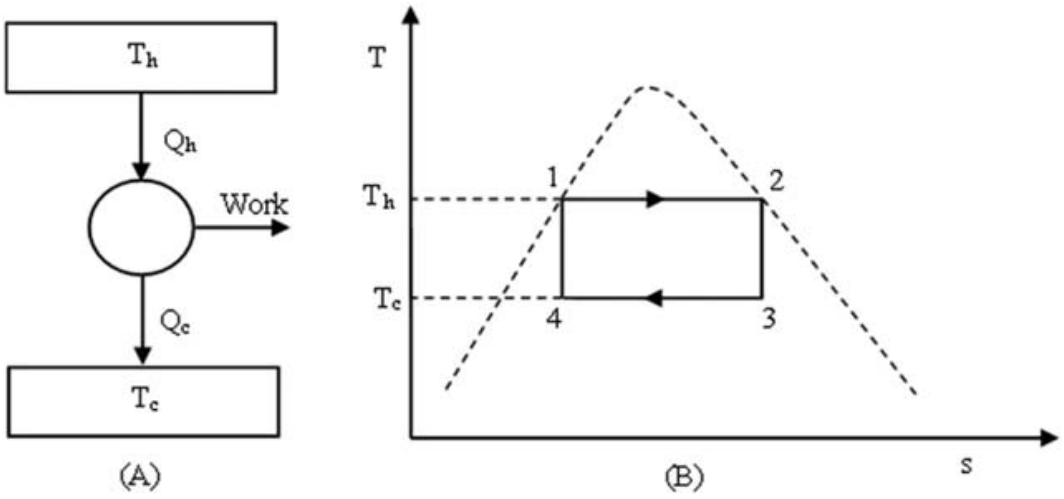

Figure 2.5: (A) Typical schematic of a Carnot machine and (B) temperature-entropy (T-s) diagram of a Carnot cycle, the dashed line represent the phase state of the fluid (the peak is the critical point of the fluid, water typically) [15].

flowing fluid. Turbomachines can be power-producing (turbines) or power-absorbing (pumps), depending on the direction of energy transfer.

The ideal Rankine cycle is composed of four processes:

1. **Process 1–2 (Isentropic Compression):** Water is first pressurized isentropically in the pump. This process requires work input (W_{pump}) and is done on a saturated liquid.

2. **Process 2–3 (Isobaric Heat Addition):** The pressurized liquid is heated at constant pressure in the solar receiver, where it evaporates to produce high-temperature, high-pressure steam. This is where the external heat (Q_{in}) is absorbed.

3. **Process 3–4 (Isentropic Expansion):** The high-pressure steam expands isentropically in the turbine, generating shaft work (W_{turbine}) for electricity production.

4. **Process 4–1 (Isobaric Heat Rejection):** The low-pressure steam finally condenses at constant pressure in the condenser, where waste heat (Q_{out}) is rejected to the environment, completing the cycle.

It is now possible to calculate the thermal efficiency of the system. The main

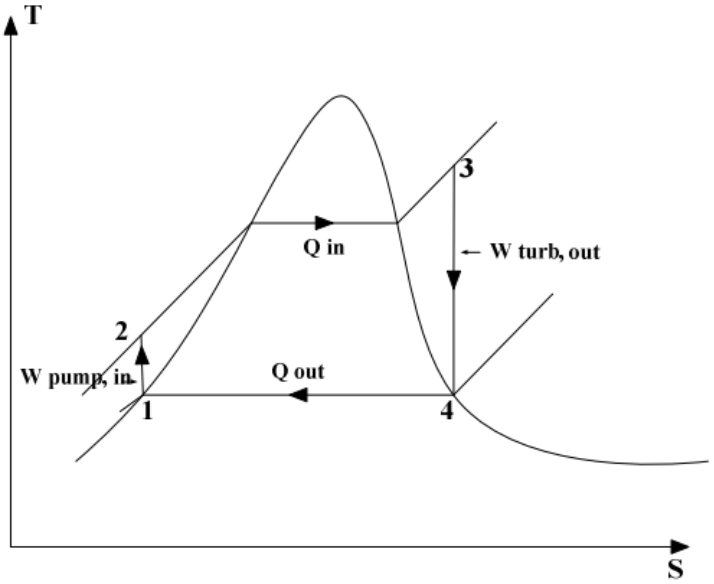

Figure 2.6: Temperature-entropy (T-s) diagram of a real Rankine cycle (W is the work, Q is the heat transferred) [24].

energy exchanges in the ideal Rankine cycle can be expressed as follows:

$$Q_{41} = \dot{m}_v(i_4 - i_1) = \dot{m}_v C_v(T_4 - T_1) \tag{2.17}$$

$$Q_{23} = \dot{m}_v(i_3 - i_2) = \dot{m}_v C_v(T_3 - T_2) \tag{2.18}$$

$$W_{12} = \dot{m}_v(i_2 - i_1) = \dot{m}_v C_v(T_2 - T_1) \tag{2.19}$$

$$W_{34} = \dot{m}_v(i_3 - i_4) = \dot{m}_v C_v(T_3 - T_4) \tag{2.20}$$

Here, C_v is the specific heat capacity of the working fluid, $\dot{m}_v$ is the mass flow rate of vapor, i is the specific enthalpy[9], and T the temperature at the

[9]In open systems, such as turbines, pumps, and heat exchangers, energy exchanges occur with a continuous mass flow across the system boundaries. Under steady-flow conditions, the total energy balance must account not only for heat and work interactions but also for the energy associated with fluid flow. For this reason, the thermodynamic potential used is the *specific enthalpy*, defined as $h = u + pv$, where u is the specific internal energy, p the pressure, and v the specific volume. Enthalpy conveniently includes the flow work term (pv), representing the energy required to push mass into or out of the control volume, thus simplifying the steady-flow energy equation $Q - W = \dot{m}(h_2 - h_1)$. For a single-phase substance with constant specific heat at constant pressure, the differential form of enthalpy is $dh = du + p\,dv + v\,dp$. From the first law for a reversible process, $\delta q = du + p\,dv$. and the definition of heat capacity $C_p = \left(\frac{\partial h}{\partial T}\right)_p$, for a reversible process at constant pressure, $\delta Q_p = dh = C_p\,dT$. Integrating between two states gives $\Delta h = C_p(T_2 - T_1)$. Hence, when pressure variations are moderate and no phase change occurs, enthalpy differences can be expressed as $h_2 - h_1 = C_p(T_2 - T_1)$, While valid for a single-phase substance with constant specific heat, it is crucial to use steam tables to determine accurate enthalpy values for processes involving phase changes [23].

indicated state points. As shown in Eq. (2.20), the turbine work output (W_{34}) increases with the turbine inlet temperature T_3. Raising T_3 through reheating or superheating the steam enhances thermodynamic efficiency and may allow the system to operate in the supercritical region.

The net work of the Rankine cycle (W_{ra}) and the corresponding thermal efficiency (η_{ra}) are defined as:

$$W_{ra} = W_{34} - W_{12} = \dot{m}_v(i_1 - i_2 + i_3 - i_4) = \dot{m}_v C_v(T_1 - T_2 + T_3 - T_4) \quad (2.21)$$

$$\eta_{ra} = \frac{W_{ra}}{Q_u} = \frac{(i_1 - i_2 + i_3 - i_4)}{(i_3 - i_2)} = \frac{(T_1 - T_2 + T_3 - T_4)}{(T_3 - T_2)} \quad (2.22)$$

Here, W is the net output work.

In practice, steam Rankine cycles in CSP plants achieve efficiencies up to 42% under subcritical conditions [25]. Reheating or superheating the steam can increase T_3 and improve efficiency, though material constraints limit the maximum operating temperature to about 900 K. Modern plants can integrate Organic Rankine Cycles, which employ low-boiling organic fluids to utilize medium and low-temperature solar or waste heat. Despite their lower efficiency compared with steam systems, they enable heat recovery and broaden the range of usable solar thermal resources.

2.5.3 Gas Turbine

The Brayton cycle is the governing thermodynamic cycle for gas turbine engines. It comprises three principal components: a compressor, a combustor (or external heater), and a turbine. Unlike the Rankine cycle which involves phase changes, the Brayton cycle uses a gas (typically air, helium, or supercritical CO_2, sCO_2) as its working fluid, which remains gaseous throughout the entire cycle. This cycle is particularly relevant for CSP systems utilizing solar towers, where operating temperatures can reach 600°C to 1000°C, allowing for higher thermal efficiencies than conventional steam cycles.

The ideal, simple Brayton cycle operates with four main processes (as shown in Figure 2.7):

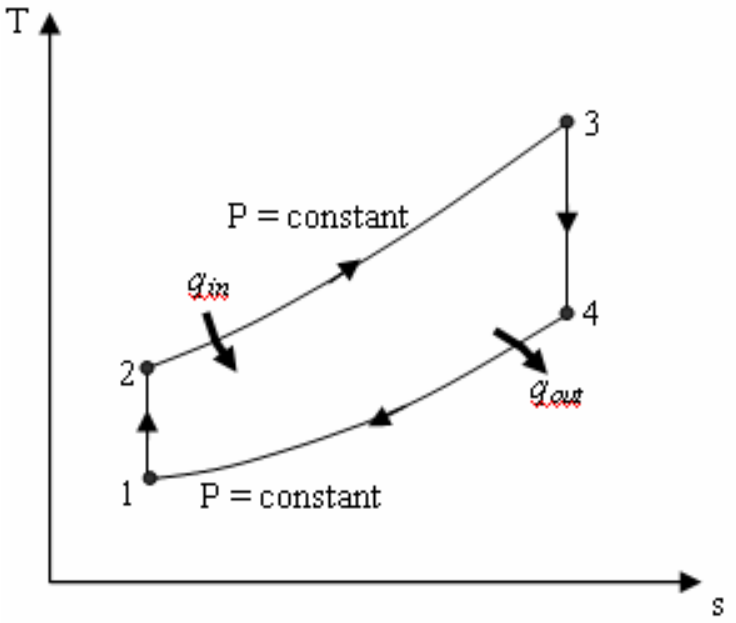

Figure 2.7: Temperature-entropy (T-s) diagram of an ideal gas turbine (P is pressure, q is heat transferred) [26].

1. **Process 1–2 (Isentropic Compression):** The working gas is compressed isentropically (at constant entropy) in a compressor, requiring work input (w_{comp}).

2. **Process 2–3 (Isobaric Heat Addition):** Heat (q_{in}) is added to the high-pressure gas at constant pressure, typically in the solar receiver or an external heat exchanger.

3. **Process 3–4 (Isentropic Expansion):** The high-energy gas expands through a turbine, producing net work output (w_{turb}).

4. **Process 4–1 (Isobaric Heat Rejection):** The gas is cooled at constant pressure in a heat exchanger (pre-cooler) back to its initial state, rejecting waste heat (q_{out}).

Energy exchanges and thermal efficiency (η_{gt}) for an ideal Brayton cycle can be expressed in terms of specific enthalpies. The work difference W_{gt} is given

by:

$$W_{12} = \dot{m}_{wf}(i_2 - i_1) = \dot{m}_{wf} C_{p,wf}(T_2 - T_1) \tag{2.23}$$

$$W_{34} = \dot{m}_{wf}(i_4 - i_3) = \dot{m}_{wf} C_{p,wf}(T_3 - T_4) \tag{2.24}$$

$$W_{gt} = \dot{m}_{wf}(i_1 - i_2 + i_3 - i_4) = \dot{m}_{wf} C_{p,wf}(T_1 - T_2 + T_3 - T_4) \tag{2.25}$$

Where $C_{p,wf}$ is specific heat capacity of the working fluid at constant pressure, T the temperature at the indicated state points and m_{wf} is the flow rate of the working fluid.
The heat supplied to the working fluid by the receiver is:

$$Q_u = Q_{23} = \dot{m}_{wf}(i_3 - i_2) = \dot{m}_{wf} C_{p,wf}(T_3 - T_2) \tag{2.26}$$

$$\eta_{gt} = \frac{W_{gt}}{Q_u} = \frac{(i_1 - i_2 + i_3 - i_4)}{(i_3 - i_2)} = \frac{(T_1 - T_2 + T_3 - T_4)}{(T_3 - T_2)} \tag{2.27}$$

This shows that higher temperature T_3 elevates the thermal efficiency.
Two general types of Brayton cycles can be distinguished:

- **Open Cycles (OCGT):** These draw atmospheric air, compress it, heat it in a solar receiver (often hybridizing with natural gas combustion), and exhaust the hot gas outside. While simple and mature, they are less efficient due to constant fluid intake and exhaust.

- **Closed Cycles (CCGT):** These operate with a fixed amount of working fluid (air, Helium, or sCO_2) which circulates continuously. Heat is added from the solar receiver. Closed cycles offer higher efficiency, allow for the use of superior working fluids, and are better suited for pure solar applications as the fluid remains clean from combustion byproducts and contained.

The Brayton cycle produces high-grade waste heat that can be recovered by integrating a Rankine or Organic Rankine cycle, with overall thermal efficiencies between 50% and 58% [27].

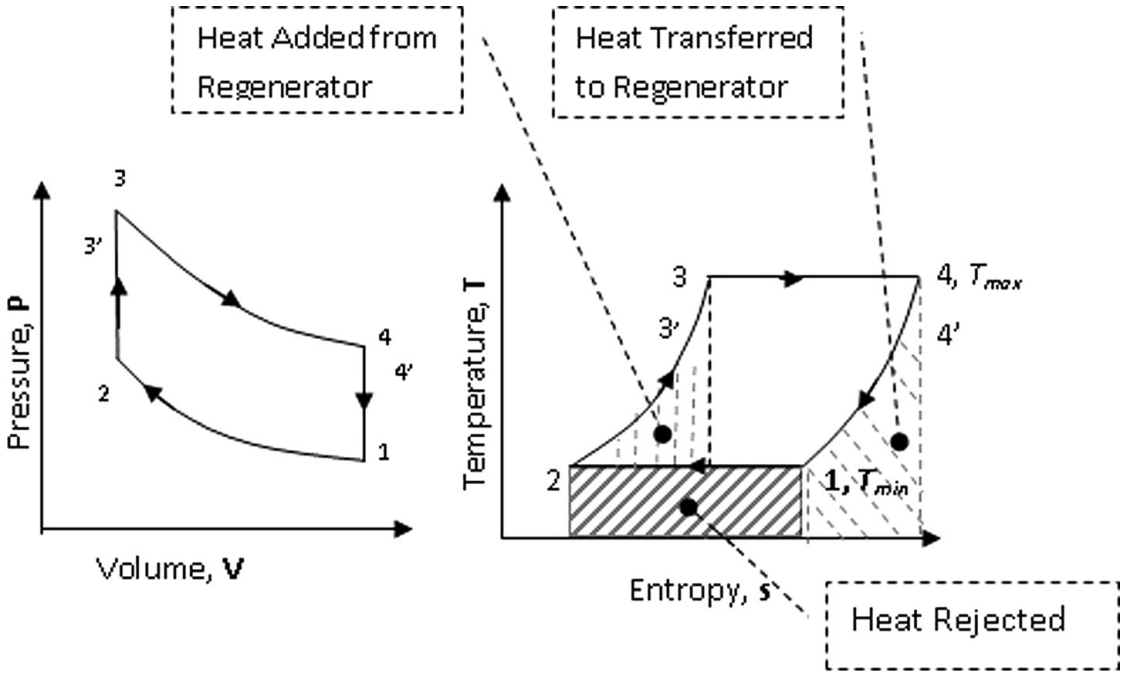

Figure 2.8: Pressure-Volume (p-V) and Temperature-entropy (T-s) diagram of an ideal Stirling cycle [28].

2.5.4 Stirling Cycle

The Stirling cycle is a highly efficient, closed-cycle regenerative heat engine cycle that is theoretically capable of achieving the maximum possible efficiency for any heat engine: the Carnot efficiency (η_{Carnot}). This makes the Stirling cycle particularly interesting for use in parabolic dish concentrator (PDC) systems, which achieve the highest concentration ratios and operating temperatures among all CSP technologies. The ideal Stirling cycle, shown in Figure 2.8, consists of four perfectly reversible processes [23] using a fixed amount of working gas (typically hydrogen or helium) within a closed volume:

1. **Isothermal Compression (Process 1–2):** The gas is compressed while in contact with the cold reservoir (T_C), and the heat (q_{out}) is rejected to the surroundings.

2. **Constant-Volume Heat Addition (Process 2–3, Regeneration):** The gas is passed through a regenerator (an internal heat storage device) where its temperature is raised from T_C to T_H at constant volume.

3. **Isothermal Expansion (Process 3–4):** The gas expands while in

contact with the hot reservoir (T_H, the solar receiver), absorbing heat (q_{in}) and producing work.

4. **Constant-Volume Heat Rejection (Process 4–1, Regeneration):** The gas passes back through the regenerator, where it cools from T_H to T_C, and the stored heat is recovered internally.

The thermal efficiency of a real Stirling cycle (which contains irreversible processes) operating between two fixed temperature reservoirs compared to the Carnot Cycle is:

$$\eta_{\text{Stirling}} = \eta_{\text{car}} \left(1 + \frac{(1-\eta_{\text{reg}}) m C_v (T_H - T_C)}{n R T_H \ln\left(\frac{V_{\max}}{V_{\min}}\right)} \right)^{-1} \tag{2.28}$$

Where C_v is the specific heat capacity of the gas at constant volume, m is the mass of the gas, n is the number of gas moles, R is the gas constant, T_c is the temperature of the cooler, T_h is the heater temperature, V_{max} is the maximum gas volume, V_{min} is the minimum gas volume, W_s is the net output work, and η_{reg} is the regenerator effectiveness. It reduces to Carnot efficiency (Eq. (2.16)) when $\eta_{reg} = 1$.

In practice, dish-Stirling systems represent the highest-efficiency CSP technology at the component level, often achieving solar-to-electric conversion efficiencies of 25% to 30%. However, the systems are complex to scale and have low compatibility with centralized thermal energy storage systems, as each dish operates as an autonomous power generation unit. Furthermore, the practical challenges in implementing the ideal cycle means that the theoretical η_{Carnot} limit is never fully achieved, but the high operating temperatures attainable make them highly efficient power producers [29].

2.5.5 Kalina Cycle

The Kalina cycle is a modified Rankine cycle designed to improve the thermal efficiency of power generation systems, particularly when dealing with medium-to-low temperature heat sources (a comparison between the two cycles is shown in Figure 2.9). It introduces a binary working fluid mixture,

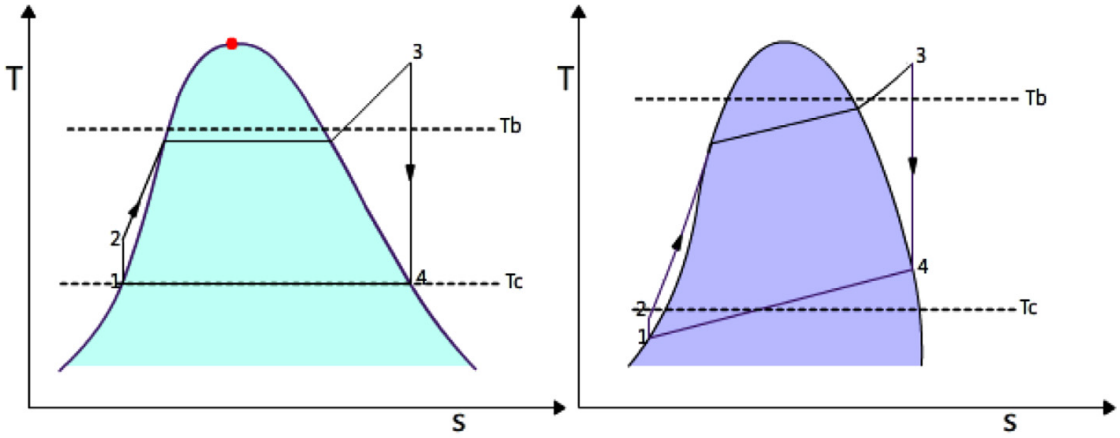

(a) T-s Diagram of Rankine cycle. (b) T-s Diagram of Kalina cycle.

Figure 2.9: Temperature-entropy (T-s) diagram comparison between (A) a real Rankine cycle and (B) a real Kalina cycle [30].

typically ammonia (NH_3) and water (H_2O), instead of a pure substance like water. The advantage of the mixture is that it boils and condenses over a range of temperatures (non-isothermally) at a constant pressure, unlike a pure fluid which changes phase at a single, constant temperature (isothermal). In other words, the effective temperature range of heat exchange is broadened, improving the cycle's thermodynamic efficiency. A simplified Kalina cycle consists of the following main components and steps:

1. **Receiver:** The ammonia–water mixture is heated by concentrated solar radiation, partially vaporizing at variable temperature and producing a two-phase mixture with ammonia-rich vapor.

2. **Turbine:** The vapor expands through a turbine to generate mechanical work (W_{turbine}). The expansion is approximately isentropic.

3. **Condenser:** After expansion, the vapor is cooled and partially condensed. Because of the varying composition, the condensation process occurs over a temperature range, improving heat recovery possibilities.

4. **Absorber/Separator:** The liquid and vapor phases are separated or mixed to restore the desired ammonia concentration before recirculation.

5. **Pump:** The liquid mixture is compressed isentropically and recirculated to the evaporator, completing the cycle.

The thermal efficiency of the Kalina cycle can always be expressed as:

$$\eta_{\text{Kalina}} = \frac{W_{\text{turbine}} - W_{\text{pump}}}{Q_{\text{in}}} \tag{2.29}$$

where Q_{in} represents the total heat absorbed in the evaporator.
Its higher efficiency arises from the non-isothermal heat addition and rejection, which minimize entropy generation during the phase-change processes. The Kalina cycle is particularly promising at medium temperatures (200°C–500°C), where pure-water Rankine systems exhibit low efficiencies. Although this technology is still under development, experimental CSP plants using Kalina cycles have demonstrated efficiency gains of 10–20%, although the complexity of managing the mixture and component corrosion remain problematic [31].

2.6 Electric generator efficiency

An electric generator is a device that converts mechanical work into electric energy. It is based on the concept of magnetic and electric induction. The efficiency of a generator (η_{gen}) is related to the energy produced (E) in comparison to the incoming net work (W_{net}) from the heat engine:

$$E = \eta_{\text{gen}} W_{\text{net}} \tag{2.30}$$

Normally, the efficiency of a generator η_{gen} is close to unity. The generator naturally produces alternating current (AC), so it doesn't require an inverter and it can be connected directly to the power grid.

2.7 Overall efficiency of a CSP system

Lastly, a final expression for the overall efficiency of the CSP system can be obtained [15].
Expressing the net work (W_{net}) as:

$$W_{\text{net}} = \eta_{\text{cycle}} \dot{Q}_u \tag{2.31}$$

where the $\dot{Q}_u = \eta_{\text{rec}} A_{ap} G_{\text{ab}}$ rewritten from Eq. (2.3) and $G_{\text{ab}} = \eta_{\text{opt}} G_{\text{ap}}$ (as in Eq.(1.23)).

Thus Eq. (2.30) can be expressed as:

$$E = \eta_{\text{opt}}\, \eta_{\text{rec}}\, \eta_{\text{cycle}}\, \eta_{\text{gen}}\, A_{ap} G_{\text{ap}} \tag{2.32}$$

$$\eta_{\text{sys}} = \eta_{\text{opt}}\, \eta_{\text{rec}}\, \eta_{\text{cycle}}\, \eta_{\text{gen}} = E/(A_{ap} G_{\text{ap}}) \tag{2.33}$$

Where η_{sys} is now the total efficiency of the system, $A_{ap} G_{\text{ap}}$ can be interpreted as the solar power imput to the concentrator.

Large-scale solar concentrators typically achieve optical efficiencies between 60% and 75%, with parabolic dish systems exceeding 85% [32]. Receiver thermal efficiency decreases as operating temperature increases. for example, it goes from about 95% at about 620 K to 83% at about 770 K [33]. This introduces a design challenge, since higher receiver temperatures reduce the fraction of absorbed solar energy converted to heat but are simultaneously required to increase the thermodynamic cycle efficiency.

In conclusion, receivers must supply heat at high temperature while remaining within material limits. Most modern CSP facilities employes steam Rankine cycles, typically achieving thermal efficiencies up to 42% and overall solar-to-electric efficiencies ranging from 8% to 35% [25]. These values highlight the need for further research and technological development to enhance CSP system performance.

CHAPTER 3

MAJOR CSP PLANTS

3 Applications in real cases

The theoretical principles presented in previous chapters can be directly observed and applied in large-scale concentrated solar power (CSP) plants. In this section, the most widespread type of CSP installations are described to illustrate how these concepts are implemented in practice, and how design decisions optimize overall plant efficiency. In the following, two types of CSP systems are presented: the parabolic trough concentrator and the solar tower, as well as modern day applications of these types of technology.

3.0.1 Parabolic Trough Concentrator

A parabolic trough concentrator (PTC) utilizes a long, curved mirror (reflector) to focus solar radiation linearly on a tubular receiver located along the focal line of the trough (Figure 3.1A). This receiver can be made up of two concentric glass tubes with a vacuum between them (an evacuated tube solar collector), and a metallic tube fitted inside the transparent concentric glass tubes [34]. The metallic tube is usually coated with a spectral selective layer to increase the absorptance of the sun radiation and reduce the thermal emissivity. The selective layers degrade in contact with air when they are hot (resulting in convection losses), therefore a vacuum inside the glass tube is applied.

The trough and receiver can move together to track the sun during the daytime, and multiple reflectors are sometimes linked together to form an array (Figure 3.1B). The solar radiation is absorbed by the metallic tube, and a heat transfer fluid, which may be oil, molten salt, or other fluid, flows through the hot metallic tube. The HTF transfers its energy to the power block where work is produced. The HTF temperatures reached are in the range of 300-400

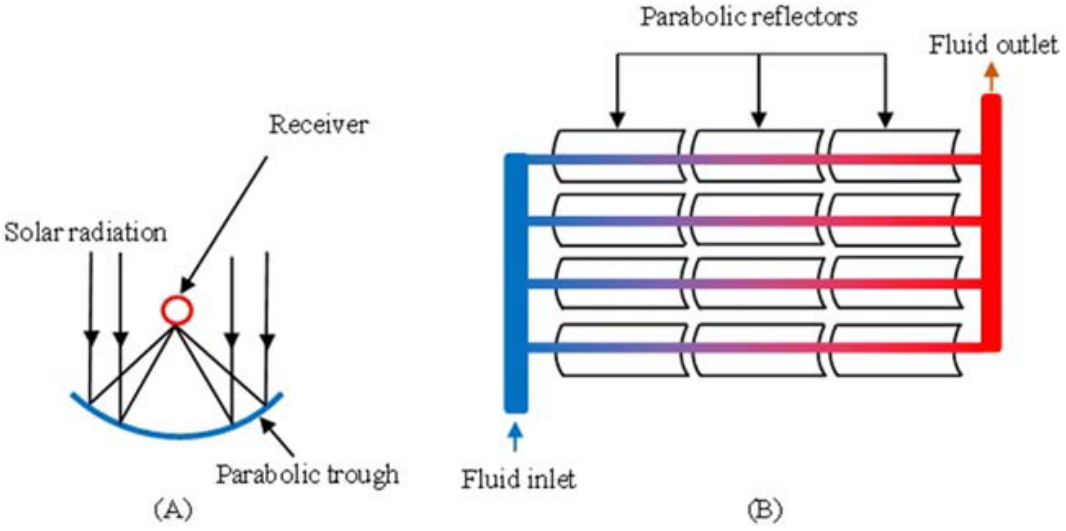

Figure 3.1: Representation of a parabolic trough concentrator. (A) shows how the beams are collected and redirected to the tubular collector, (B) shows multiple units of PTC connected to the same HTF mechanism [15].

°C, and the thermodynamic cycle used prevalently is the Rankine cycle. The PTC system is cheap and easy to manufacture and it can be accompanied with a thermal energy storage, but it has a low concentration ratio, thus achieving medium operating temperatures [10]. Nonetheless, this range of temperature is satisfactory for powering the steam turbine. It offers an initial low investment for a simple design.

3.0.2 Solar Tower

In a solar tower, a field of large mirrors is employed to focus incident solar radiation to a point-like receiver mounted on top of the tower (Figure 3.2), where it is converted to heat. These large mirrors, also called heliostats, track the sun individually in two axes. The most common type of receiver used is a cylindrical arrangement of panels made of many parallel tubes (external tubular receiver). The concentrated sunlight from the heliostat field is focused onto the outer surface of these tubes, transferring energy to the heat transfer fluid inside. This type of receiver has a substantial heat loss because of the high temperature reached, and significant thermal stress of the materials caused by the non-uniform heat transfer [35].

Then the HTF transfers its energy to the power block. The HTF utilized are

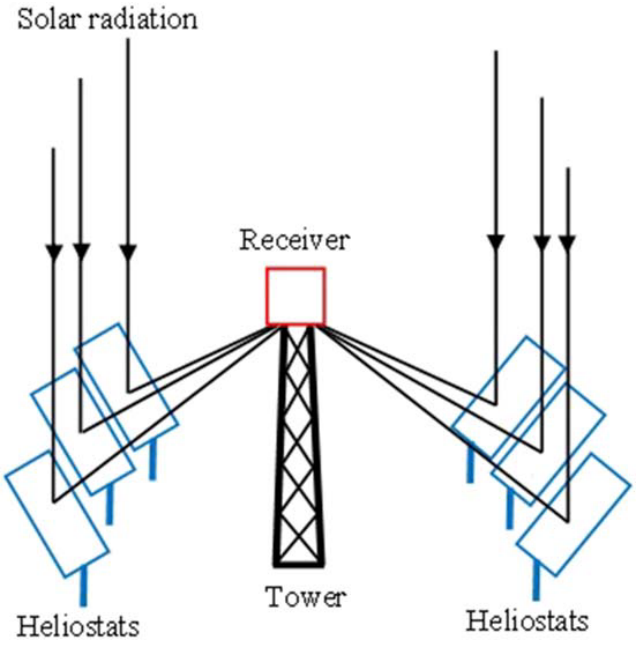

Figure 3.2: Representation of a solar tower and how solar beams are redirected to the point like receiver [15].

molten salts, though other type of HTF can be used depending on the type of heat engine and the Rankine cycle is the primary thermodynamic cycle for converting heat to work.

A high amount of solar radiation is reflected by the mirrors onto the receiver, in view of this, the ST technology can achieve higher temperatures (in the range of 500-565 °C) than the PTC and possibly be exploited in the gas turbine technology [36]. Moreover, high temperatures render the use of thermal storage with molten salt attractive [37]. The project implementation requires higher capital investment than the PTC technology, but it's overall more efficient in solar collection and in land usage.

3.1 Noor Ouarzazate Complex, Morocco

The Noor Ouarzazate complex is one of the largest operational solar facilities in the world [38]. The facility is divided into four complexes (Noor I,II,III,IV); three of these utilize concentrated solar power (CSP) technology. The Noor I and II employ parabolic trough concentrator systems. The Noor III uses solar tower technology. The complex has a total capacity of 510 MW, one of the biggest in the world.

3.1.1 Solar Resource and Tracking

Located in southern Morocco, the site receives a high annual DNI of approximately 2,200 kWh/($m^2 \cdot$ year). The parabolic trough systems use a single axis tracking system, while the solar tower system uses a dual-axis tracking to maintain high optical efficiency, ensuring the absorbed solar energy is maximized throughout the day.

3.1.2 Noor I-II

The Noor I is an example of parabolic trough concentrator, with an installed capacity of 160 MW, integrated with evacuated tube receivers. The heat transfer fluid used in the receiver is a synthetic oil, Dowtherm A (which is a similar composition to Therminal VP). Molten salts (specifically Solar Salt) are used to store the excess heat in a two-tank system (with a separation between the hot and cold storage fluids, which minimizes heat loss and thermal degradation) indirect system (meaning that it's not using the same storage fluid as the HTF) with a capacity of 3 hours. The choice of molten salt balances high thermal capacity with manageable viscosity to minimize pumping power while maintaining turbulent flow for efficient convective heat transfer. The thermal cycle used is a conventional Rankine Cycle, with a wet cooling system. The overall gross thermal-to-electric conversion efficiency of the Noor I CSP plant is typically within the range of 10-25%. The reported annual production is 370 GWh with a cost per electricity of 0.18 $/kWh. These numbers can be used to simulate a case scenario for the properties of the plant [39]. The results estimate a design point DNI of 1003 W/m^2, with a gross output of 177.78 MW, with a heat storage temperature 292 °C (cold tank) and 368 °C (hot tank).
The Noor II has been built with similar components and has a nominal capacity of 200 MW, but it incorporates a new generation of parabolic trough components. It also uses a dry cooling method (air) to reduce water usage. The thermal energy storage also collects more thermal energy, with a duration of about 7 hours.

Figure 3.3: Image of parabolic trough concentrators system in the complex of Noor I [40].

3.1.3 Noor III

The design of Noor III is a solar tower with a capacity of 150 MW [38]. Thousands of mirrors are installed on platforms supported by columns, and direct sunbeam to an external cylindrical tube located on a 250 m tall tower. It reaches higher temperature than its PTC counterparts. The HTF used thus needs to withstand higher temperatures, so molten salts (specifically Solar Salt) are used as the heat transfer fluid as well as for the thermal energy storage with a capacity of 7-7.5 hours (a dual tank system where the hot tank is at 565°C, the cold tank at 290°C). The choice of molten salt has the same considerations for the thermal energy storage used for the Noor PTC systems. The thermal cycles used is a conventional Rankine Cycle capable of higher efficiency due to the higher reached temperature. The heated molten salt is delivered to a Rankine cycle steam turbine. Thermal storage enables dispatchable electricity generation, illustrating the practical relevance of cycle efficiency analysis. Reported overall plant efficiency ranges between 25-35%, which is consistent with theoretical predictions when accounting for optical and thermal losses [41]. A 10-day reliability test was conducted to demonstrate its ability to generate continuous electricity even in the absence of sunlight.

Figure 3.4: Solar tower of the Noor III unit. The photo was taken with a negative film [38].

3.2 Mohammed bin Rashid Al Maktoum Solar Park, UAE

This solar park has been built in multiple phases, each utilizing different solar energy technologies. The phase 4 presents a CSP generation complex, also called Noor Energy 1, and is located in Saih Al-Dahal, in the United Arab Emirates [42]. It presents 4 units of CSP, 3 of which are parabolic trough technology (each with a capacity of 200 MW) and 1 unit composed of a solar tower (generating 100 MW), with a total capacity of 700 MW, the largest in the world up to now. It combines both parabolic trough and solar tower technologies, with Dowtherm A being used as the HTF in the parabolic trough units and molten salt (Solar Salt) as the primary HTF in the solar tower and as well as the energy storage shared medium [43]. This project has reached an all time low for cost to electric production of \$0.073/kWh in comparison with other relevant modern CSP systems. This very competitive price was obtained through a good financial condition and improved technologies.

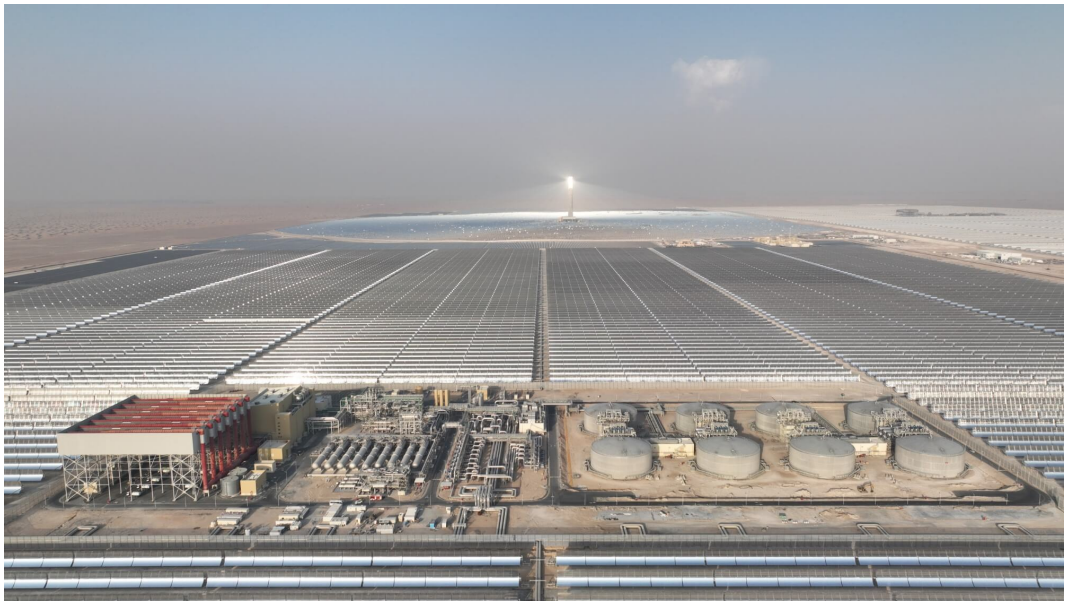

Figure 3.5: Image representing parabolic trough unit mirrors of Noor Energy 1 complex collecting solar radiation [44].

3.2.1 Solar Resource and Tracking

The Noor Energy 1 site has an estimated value of annual receiving DNI of 1.900 kWh/($m^2 \cdot$ year), a typical value for desert areas in the sunbelt zone. The parabolic trough units uses a single tracking system that moves from east to west and the solar tower system heliostats use dual-axis tracking to maintain high optical efficiency.

3.2.2 Parabolic Trough units

The type of receiver used in the PTC units is vacuum-insulated tubes that run along the focal line of the mirrors. An image of a PTC unit is presented in Figure 3.5.

The HTF used by each PTC units is a synthetic oil (similar composition of Therminol VP-1), which transfers its energy either to the power generation unit or in a molten salt storage (Solar Salt), shared across all 4 units, including the solar tower. This provides a total of 15 h of continuous power generation. The power block uses a standard Rankine cycle with water/steam as the medium. The operational system is presented in Figure 3.6. The HTF flow in a turbulent flow regime during the normal operation, to enhance mixing

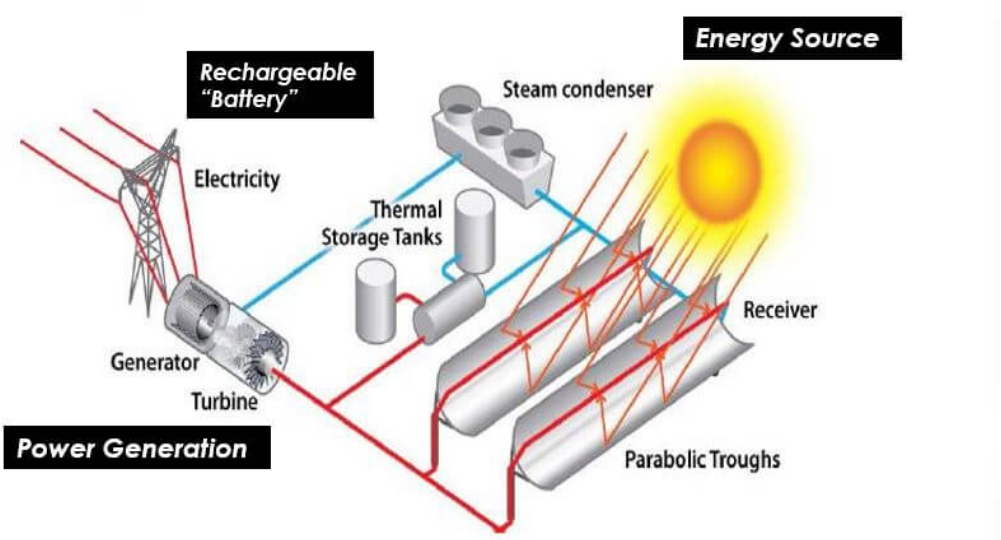

Figure 3.6: Design structure that had been utilized to build the Noor Energy 1 PTC units [44].

and convective heat transfer, minimizing thermal gradients and ensuring uniform heat distribution. It's estimated radiation to energy conversion efficiency falls into the typical for a parabolic through system: 15% to 25% [45].

3.2.3 Solar Tower unit

The tower holds the title for the tallest CSP tower at 263 m. It's surrounded by 70,000 large, dual-axis tracking mirrors (heliostats) that focus sunlight onto a receiver at the top. An image of the heliostats and the solar tower is shown in Figure 3.7.

The receiver is an external type: 1,000 thin metal tubes arranged in vertical panels where the HTF, Solar Salt, is conveyed and heated. Because of the high temperature reached over (560°C) Solar Salt is used as HTF and as well as the direct fluid energy storage in the shared two tanks storage system (the hot tank is at 565°C and the cold tank is at 290°C). The stored thermal energy allows continuous electricity generation, demonstrating the integration of HTF properties with the used Rankine cycle efficiency. The design achieves reported overall efficiencies of 25-35%, illustrating the validity of combining theoretical and practical considerations [41]. A schematic of the design of the structure and the components are illustrated in Figure 3.8.

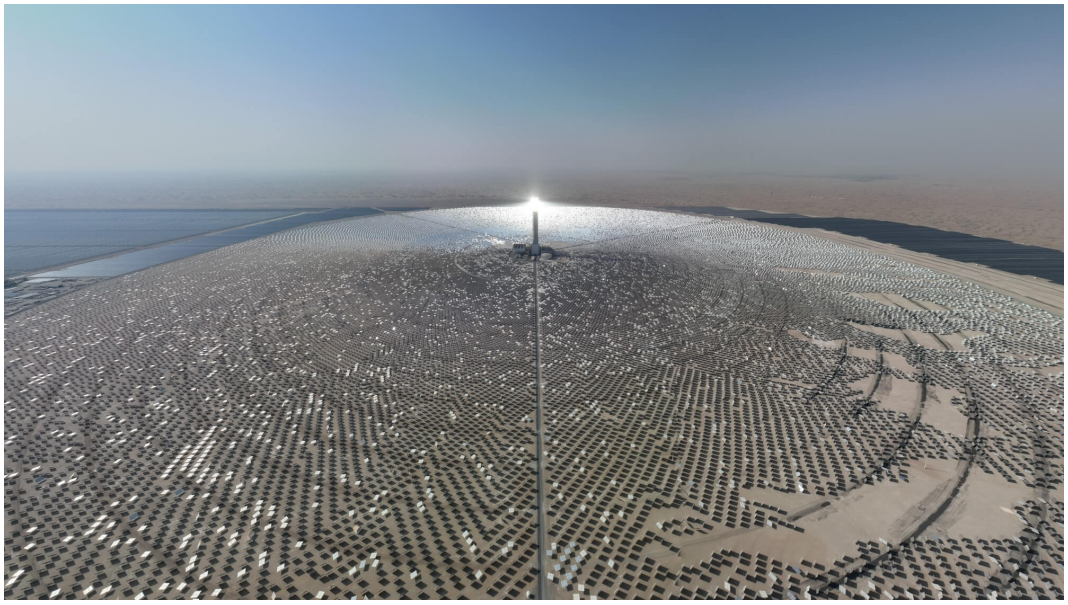

Figure 3.7: Image of the solar tower with the heliostats field of Noor Energy 1 [44].

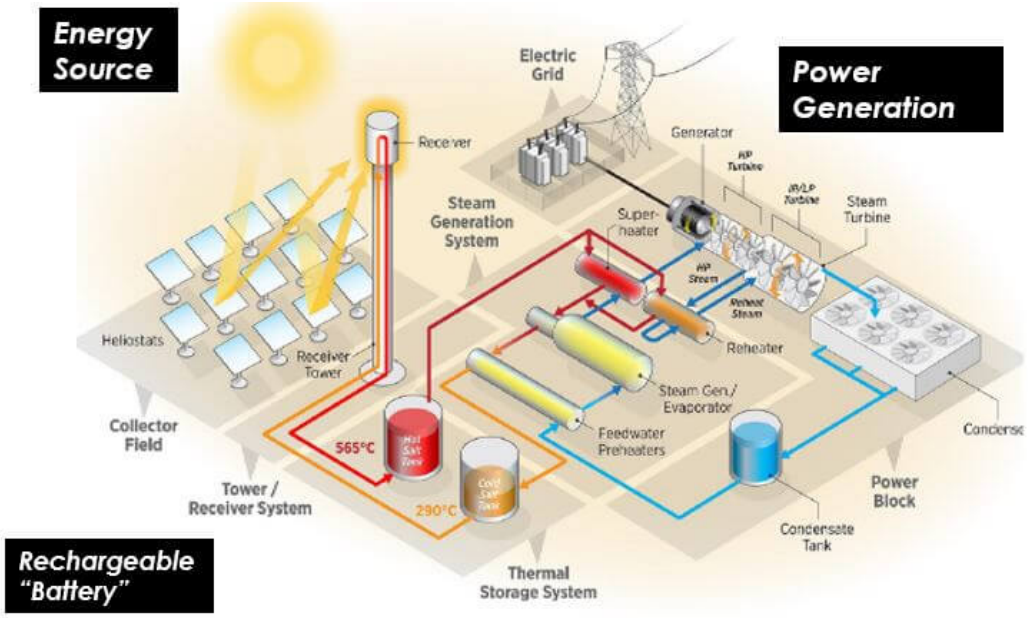

Figure 3.8: Design structure utilized to build the Noor Energy 1 solar tower system [44].

3.3 Future prospects

As introduced, the PTC and Solar Tower with the Rankine cycle power generation technologies are very reliable and mature in modern day application. Other type of CSP technologies are under study, where sometimes theoretically can offer higher efficiency, but their cost and material factors are the limiting practical parameters. A comparison with production and competitive cost with other form of energy production should also be taken into consideration for future prospect of the CSP technology.

3.3.1 Economic competitiveness of CSP

LCOE COMPARISON		
Energy Source	Range ($/kWh)	Notes
New Onshore Wind	$0.033 - $0.034	Highly competitive and often the cheapest new source.
New Utility-Scale Solar PV	$0.040 - $0.049	Very competitive and widespread.
New Natural Gas Plant	$0.048 - $0.109	Varies widely based on fuel costs.
Coal	$0.071 – $0.173	Generally the most expensive new generation source.
Nuclear	$0.112 – $0.189	High capital costs and long construction times make it very expensive.
Hydropower	$0.057 – $0.08+	Variable based on project size, location, and infrastructure.
Geothermal	$0.060 – $0.102	Stable, costs depend on the quality and accessibility of the geothermal resource.
Current CSP	$0.09 - $0.18	Generally higher than PV/wind, but offers dispatchability.

Table 2: LCOE of current energy resources [46].

A good comparison for cost production is the Levelized Cost of Energy

(LCOE) between different forms of energy production. Levelized Cost of Energy is the average cost of producing one unit of electricity over a plant's lifetime, accounting for all capital, operating, and fuel expenses divided by the total energy generated.

An interesting fact is that another type of solar energy production, the photovoltaic technology (PV) has reached a point of maturity where the costs of production are extremely competitive, thus most CSP plants present a PV section to integrate both technology advantages: the PV[10] offers a lower cost of production, while the CSP meets the peak demand of energy when sunlight is not present. For CSP plants the target to become even more widespread as viable resource is between \$0.04 - \$0.07/kWh. The LCOE of various form of energy production is show in Table 2.

3.4 Possible future applications

This section gives a overview on less relevant CSP plants, specially in large-scale power production, and how could some theoretical aspect become a future application.

3.4.1 Linear Fresnel Reflector

A Linear Fresnel Reflector (LFR) system consists of many flat or slightly curved mirror strips on each side of a tubular receiver [47], as shown in Figure 3.9. It conveys sun rays in a line with a relatively low concentration ratio, thereby resulting in lower operational temperature and uses a single axis tracking system. One drawback of this system is the shading effect between adjacent reflectors, which led to the development of a compact linear Fresnel reflector (CLFR) [48]. In the CLFR system, adjacent mirrors are oriented toward different absorber tubes located in opposite directions, therefore reducing some of the shading drawbacks and the size of land required by the solar field.

[10]Photovoltaic (PV) technology converts solar radiation directly into electrical energy through the photovoltaic effect, in which photons generate electron–hole pairs within a semiconductor junction. Unlike CSP systems, PV modules have no moving parts and do not rely on thermal processes, resulting in high modularity and low operating costs, but they lack the inherent thermal storage capability that enables dispatchable power generation.

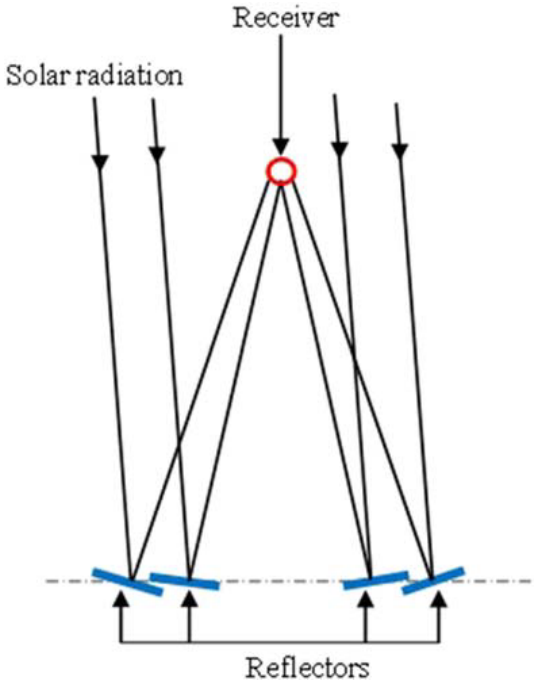

Figure 3.9: Schematics of a linear Fresnel reflector. Sun rays convergence on a tubular like receiver after being reflected. It's notable also the shading effect between consecutive mirrors [15].

The most commonly utilized HTF fluids are synthetic oils, but also water can be used (as a direct HTF, which means is used also as the working fluid in the heat engine), or even molten salt. A thermal energy storage can also be associated. One advantage of the system is that it's a cheaper initial investment compared to other CSP counterparts because of its simpler structure. Conventionally a Rankine cycle is used, but to further optimally extract energy from the low HTF working temperature a Kalina cycle with the mixture of water and ammonia can be theoretically employed [49]. The total predicted efficiency for the plant is between 15% to 19%.

3.4.2 Parabolic Dish Concentrator

A Parabolic Dish Concentrator (PDC, also known as a Parabolic Dish Stirling system because the thermodynamic cycle conventionally integrated is a Stirling cycle) uses large curved mirrors to focus solar radiation on a point-like focal receiver above the reflector (as shown in Figure 3.10). To optimally suntrack the incoming beam, the reflector and the receiver move together [10]. This

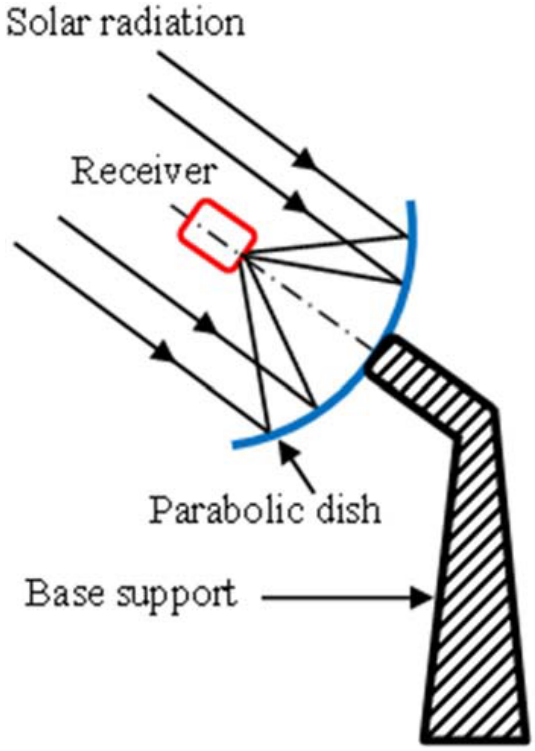

Figure 3.10: Representation of the sun beams convergence in a point like receiver on a parabolic dish stirling system [15].

configuration allows to reach very high temperatures in the range of 400°C and 1000°C, therefore the HTF commonly used are molten salt or gases and the commonly associated thermal cycle is the Stirling cycle, which is suited for the high temperatures and some prototypes are built with the Brayton cycle. The heat engine is mounted directly on the receiver, limiting heat losses and cooling needs. Among the different types of CSP technologies, the PDC exhibits the highest thermodynamic efficiency (according to the Carnot limit), but it produces electricity at the highest cost. Another drawback of this type of CSP technology is its low compatibility with thermal storage [48]. PDCs have low capacity of power (in the order of kW or less), with each dish generating electricity autonomously and brings to the implication that thousands of dishes are required to build a largescale power plant, making them instead suitable for medium to small energy production plants.

3.4.3 Solar Tower with Gas Turbine

As mentioned, solar towers (and also parabolic dish concentrators) are capable of reaching higher temperatures compared to other CSP counterparts, making them suitable for gas turbine engine (Brayton cycle), specifically the closed cycle gas turbine (to avoid heat dispersion in the open cycle). Theoretically, the most efficient working fluid expected to operate at those temperatures is the supercritical CO_2, compared to other gases in CSP systems. Its main advantages are [50]:

- **Reduced Compression Work**: The cycle can be designed so that the compressor inlet operates very close to the critical point (31.1°C and 73.8 bar), where sCO_2 has a very high density, similar to a liquid. Compressing a dense fluid requires significantly less energy (work) than compressing a less dense gas like air, helium, or nitrogen. This would increase the net power output from the plant and increasing overall cycle efficiency.

- **Comparable Efficiency at Lower Temperatures**: The sCO_2 cycle can achieve thermal efficiencies of around 48-50% at turbine inlet temperatures of 500-600°C, a range where a helium cycle would require much higher temperatures (up to 850°C) to reach similar efficiency levels.

- **Low Critical Point**: The critical point of CO_2 is easily accessible (around ambient temperature and manageable pressure), making the system technically feasible and economically viable.

- **Chemical Stability**: CO_2 is a non-toxic, non-flammable, and chemically stable compound that does not corrode materials as aggressively as water/steam might at extreme temperatures, though material challenges at ultra-high temperatures still exist.

- **Water-Free Cooling**: The cycle can utilize dry cooling systems (air cooling) without the severe efficiency penalties seen in conventional steam

cycles, which is a major advantage for applications in arid or desert regions, such as CSP plants.

3.5 Comparison between CSP technologies

A final comparison between the data used on the current CSP technologies is shown in table 3.

Modern CSP systems have reached technological maturity, particularly in

CSP TECHNOLOGY COMPARISON				
Technology	Temperature	HTF	Storage	Typical Efficiency
PTC	300–400°C	Oil	Yes	15–25%
ST	500–565°C	Molten salt	Yes	25–35%
LFR	250–350°C	Oil / Steam	Limited	15–19%
PDC	400–1000°C	Gas	No	13-32%

Table 3: Comparison data between different types of CSP technology.

parabolic trough and solar tower configurations. Their integration with thermal energy storage enables dispatchable renewable power, though economic competitiveness remains a challenge relative to photovoltaic systems.
Applications of LFR and PDC for large scale energy production are not widespread. The lower optical efficiency and limited operating temperature restrict the overall performance of LFR, while scalability limitations with difficult thermal storage integration make PDC less suitable for utility-scale power generation. The performance differences across CSP technologies are primarily linked to their optical configuration, achievable operating temperature, and the corresponding thermodynamic cycle efficiency. Higher temperatures lead to higher Carnot efficiencies, but also impose stricter material and heat-loss constraints.

Current research is focusing on new combinations of optical systems, high-temperature receivers, advanced heat-transfer fluids and alternative power cycles (such as supercritical CO_2 Brayton cycles). These developments aim to increase operating temperatures, reduce thermal losses, and improve overall system efficiency while maintaining economic competitiveness.

Conclusion

This thesis has examined the fundamental physical principles and technological implementations that enable Concentrated Solar Power (CSP) systems to convert solar radiation into dispatchable electrical energy. Beginning with the description of solar resource characteristics and the mechanisms of optical concentration, the work has outlined how CSP plants exploit geometrical optics, radiative transfer, and thermodynamic conversion to achieve high-temperature operation suitable for efficient power generation.

In particular, for each stage of the energy conversion chain, a method to quantify the efficiency has been defined leading to an overall evaluation of the solar-to-electric conversion efficiency. This efficiency depends on the type of CSP concentration structure used, the geometry of the receiver and the Heat Transfer Fluid (HTF) used, the thermodynamic cycles employed, as well as some final considerations on the electric generator efficiency. Furthermore, the physical characteristics required for HTFs to enhance receiver performance have been discussed, together with the application of the Navier-Stokes equation to describe the fluid behaviour during heat transfer processes. To convert heat into mechanical work, different thermodynamic cycles have been compared with their theoretical conversion efficiency under ideal operating conditions.

The theoretical aspects have been complemented with real case studies, analyzing widely deployed CSP configurations like Parabolic Trough Collectors (PTC) and Solar Towers (ST) and illustrating how they are implemented in large plants like Noor Complex in Morocco and Noor Energy 1 in the United Arab Emirates. A global comparison with other forms of energy production has been provided in terms of Levelized Cost of Energy (LCOE). Additionally, other less common technologies have been examined such as Linear Fresnel Reflectors (LFR) and Parabolic Dish Concentrators (PDC), outlining their specific advantages and limitations.

These considerations pave the way for future research aimed at increasing and maximizing overall system efficiency, including the development of advanced high-temperature cycles such as the sCO_2 Brayton cycle.

Bibliography

[1] C. Julian Chen. *Physics of Solar Energy*. John Wiley & Sons, 2011. ISBN: 9780470647806.

[2] E.-H. Kim, Y.-G. Park, and J. H. Roh. "Competitiveness of open-cycle gas turbine and its potential in the future Korean electricity market with high renewable energy mix". In: *Energy Policy* 129 (2019). DOI: 10.1016/j.enpol.2019.03.014.

[3] International Energy Agency. *Data and statistics*. https://www.iea.org. Visited: 04-11-2025. 2020.

[4] R. P. Kane. "Sun-Earth relation: Historical development and present status - a brief review". In: *Advances in Space Research* 35 (2005). DOI: 10.1016/j.asr.2005.03.142.

[5] Robert L. Jaffe and Washington Taylor. *The Physics of Energy*. Cambridge: Cambridge University Press, 2018. ISBN: 978-1107016651.

[6] U.S. Energy Information Administration. *International Energy Annual 2004*. U.S. Department of Energy, Energy Information Administration. Visited: 10-11-2025. 2004. URL: https://www.eia.gov/outlooks/iea/archived/2004/.

[7] Solargis. *Solar resource maps of world: Direct normal irradiation*. https://solargis.com/maps-and-gis-data/download/world. Visited: 29-10-2025. 2019.

[8] M Kotti, A Argiriou, and A Kazantzidis. "Estimation of direct normal irradiance from measured global and corrected diffuse horizontal irradiance". In: *Energy* 70 (2014).

[9] Zhifeng Wang. *Design of Solar Thermal Power Plants*. London, Uk: Academic Press, 2019. ISBN: 9780128156131.

[10] H. L. Zhang et al. "Concentrated solar power plants: Review and design methodology". In: *Renewable and Sustainable Energy Reviews* 22 (2013). DOI: 10.1016/j.rser.2013.01.032.

[11] John A. Duffie and William A. Beckman. *Solar Engineering of Thermal Processes*. 4th. Hoboken, NJ: John Wiley & Sons, 2013. ISBN: 9780470873663.

[12] Sabah Auda Abdul Ameer and Haroun A. K. Shahad. "Characteristics review of optical concentrators". In: *International Journal of Current Engineering and Technology* 7 (1 2017), pp. 169–171.

[13] A. Rabl. "Comparison of solar concentrators". In: *Solar Energy* 18.2 (1976), pp. 93–111. DOI: 10.1016/0038-092X(76)90043-8.

[14] Vasili Karneichyk. *Mastering Optical Invariants: Key Principles in Optical System Design*. https://www.opticsforhire.com/blog/optical-system-invariants. Visited: 18-11-2025. 2024.

[15] Amos Madhlopa. *Solar receivers for thermal power generation : fundamentals and advanced concepts*. Amsterdam, Netherlands: Elsevier, 2022. ISBN: 9780323852722.

[16] Zuriel Aquino-Santiago et al. "Enhancing the Thermal Efficiency of Parabolic Trough Collectors by Using Annular Receivers for Low-Enthalpy Steam Generation". In: *Processes* 12.12 (2024). ISSN: 2227-9717. DOI: 10.3390/pr12122653.

[17] Collins Chike Kwasi-Effah. "Heat Transfer Fluids in Solar Thermal Power Plants". In: *Journal of Science and Technology Research* 1.10 (2024).

[18] Frank P. Incropera et al. *Fundamentals of Heat and Mass Transfer*. John Wiley & Sons, 2013. ISBN: 978-0470501979.

[19] ASHRAE American Society of Heating, Refrigerating and Air-Conditioning Engineers, Inc. *ASHRAE Handbook - Fundamentals*. Atlanta, GA, USA: ASHRAE (American Society of Heating, Refrigerating and Air-Conditioning Engineers, Inc.), 2017. ISBN: 978-1-939200-57-0 (I-P Edition).

[20] Wikipedia contributors. *Navier–Stokes equations*. https://en.wikipedia.org/wiki/Navier-Stokes_equations. Visited: 13-11-2025. 2025.

[21] Henk Kaarle Versteeg and W Malalasekera. *An introduction to computational fluid dynamics: the finite volume method*. Pearson Education, 2007.

[22] Alberto Giaconia et al. “Assessment and Perspectives of Heat Transfer Fluids for CSP Applications”. In: *Energies* 14.22 (2021), p. 7486. DOI: 10.3390/en14227486.

[23] Sergio Focardi et al. *Fisica generale: meccanica e termodinamica*. 2nd ed. CEA (Casa Editrice Ambrosiana), 2014. ISBN: 9788808182159.

[24] Balaram Saha, Vivek Patel, and Kalyan Chatterjee. “Assessment of process parameter to improving power plant performance”. In: Nov. 2014, pp. 441–446. DOI: 10.1109/CIPECH.2014.7019125.

[25] F. Petrakopoulou et al. “Assessing the performance of a solar-assisted power plant using supercritical fluid cycles”. In: *Applied Thermal Engineering* 112 (2017), pp. 1453–1463. ISSN: 1359-4311. DOI: 10.1016/j.applthermaleng.2016.07.168.

[26] Ezenwa Alfred Ogbonnaya and Ugwu Hyginus Ubabuike. “Analysis of steam recuperative system to cogas plant”. In: 7 (May 2012).

[27] A. Poullikkas. “An overview of current and future sustainable gas turbine technologies”. In: *Renewable and Sustainable Energy Reviews* 9 (2005), pp. 409–443. DOI: 10.1016/j.rser.2004.05.009.

[28] Dhananjay Thombare and Suhas Karmare. “Theoretical and experimental investigation of Alfa type bio mass Stirling engine with effect of regenerator effectiveness, heat transfer, and properties of working fluid.” In: *Journal of Renewable and Sustainable Energy* 4 (Jan. 2012), pp. 1–14.

[29] K. Mansiri, S. Sukchai, and C. Sirisamphanwong. “Investigations to conduct a study about possibilities to use small scale solar dish Stirling engine system in Thailand”. In: *Energy Procedia* 52 (2014), pp. 307–316. ISSN: 1876-6102. DOI: 10.1016/j.egypro.2014.07.081.

[30] Hussam Jouhara et al. “Waste Heat Recovery Technologies and Applications”. In: *Thermal Science and Engineering Progress* 6 (Apr. 2018). DOI: 10.1016/j.tsep.2018.04.017.

[31] Anish Modi et al. “Thermoeconomic optimization of a Kalina cycle for a central receiver concentrating solar power plant”. In: *Energy Conversion and Management* 115 (2016), pp. 276–287.

[32] A. Kribus. “Concentrated Solar Power: Components and materials”. In: *EPJ Web of Conferences* 148 (2017), p. 00009. DOI: 10.1051/epjconf/201714800009.

[33] Manuel J. Blanco and Lourdes Ramirez Santigosa, eds. *Advances in Concentrating Solar Thermal Research and Technology*. Duxford, UK: Woodhead Publishing, an imprint of Elsevier, 2017. ISBN: 978-0-08-100517-0.

[34] María Elena Carra et al. “Study of parameters influence on the measurement of vacuum level in parabolic trough collectors’ receivers using infrared thermography”. In: *Infrared Physics & Technology* 131 (2023), p. 104657. DOI: 10.1016/j.infrared.2023.104657.

[35] Giancarlo Gentile et al. “Enhancing solar tower competitiveness with star-shaped receivers”. In: *Applied Energy* 391 (2025), p. 125844. ISSN: 0306-2619.

[36] Amos Madhlopa and Edmund Okoroigwe. “Solar gas turbine systems”. In: *Encyclopedia of Sustainable Technologies*. Ed. by Martin A. Abraham. Elsevier, 2017. ISBN: 9780128046777. DOI: 10.1016/B978-0-12-409548-9.10150-2.

[37] Giuseppe Franchini et al. “A comparative study between parabolic trough and solar tower technologies in Solar Rankine Cycle and Integrated Solar Combined Cycle plants”. In: *Applied Thermal Engineering* 51.1-2 (2013). DOI: 10.1016/j.applthermaleng.2012.09.022.

[38] Wikipedia contributors. *Ouarzazate Solar Power Station*. https://en.wikipedia.org/wiki/Ouarzazate_Solar_Power_Station. Visited: 13-11-2025. 2025.

[39] Aabla Yahya et al. “Parabolic Trough Plant Performance In Morocco For Techno-economic Evaluation: A Case Study Of Noor 1”. In: July 2024. DOI: 10.1109/ECAI61503.2024.10607532.

[40] Focus. *Energia Come funziona Noor, il più grande impianto solare termodinamico del mondo*. https://www.focus.it/scienza/energia/noor-piu-grande-impianto-solare-termico-del-mondo. Visited: 16-11-2025. 2016.

[41] R. P. Merchán et al. "High temperature central tower plants for concentrated solar power: 2021 overview". In: *Renewable and Sustainable Energy Reviews* 155 (2022), p. 111892. ISSN: 1364-0321. DOI: 10.1016/j.rser.2021.111892.

[42] Wikipedia contributors. *Mohammed bin Rashid Al Maktoum Solar Park*. https://en.wikipedia.org/wiki/Mohammed_bin_Rashid_Al_Maktoum_Solar_Park. Visited: 14-11-2025. 2025.

[43] Dubai Electricity and Water Authority (DEWA). *Integrated Report for the Year 2021*. https://www.dewa.gov.ae/-/media/Images/Investor-Relations/Integrated-reports/AR/Integrated_report_for_the_year_2021.ashx. Visited: 16-11-2025. 2022.

[44] Noorenergy. *Technologies*. https://noorenergy.ae/technologies. Visited: 16-11-2025. 2025.

[45] Latifa Sabri and Mohammed Benzirar. "Determination of the Maximum Efficiency of Concentrated Solar Power (Parabolic Trough and Central Tower) using A Genetic Algorithm". In: *Asian Journal of Applied Sciences* 3 (2 2015). URL: https://www.ajouronline.com/index.php/AJAS/article/view/2526.

[46] International Renewable Energy Agency (IRENA). *Renewable Power Generation Costs in 2024*. Tech. rep. Abu Dhabi: IRENA, 2025. URL: https://www.irena.org/-/media/Files/IRENA/Agency/Publication/2025/Jul/IRENA_TEC_RPGC_in_2024_2025.pdf.

[47] Ugo Pelay et al. "Thermal energy storage systems for concentrated solar power plants". In: *Renewable and Sustainable Energy Reviews* 79 (2017). DOI: 10.1016/j.rser.2017.03.139.

[48] David Barlev, Ruxandra Vidu, and Pieter Stroeve. “Innovation in concentrated solar power”. In: *Solar Energy Materials and Solar Cells* 95.10 (2011). DOI: 10.1016/j.solmat.2011.05.020.

[49] Jianyong Wang et al. “Optimum Control Strategy for a Low-Temperature Solar Kalina Cycle Power Generation Under Off-Design Conditions”. In: Nov. 2017, V006T08A007. DOI: 10.1115/IMECE2017-70064.

[50] Michel Molière et al. “Supercritical CO2 Power Technology: Strengths but Challenges”. In: *Energies* 17.5 (2024). DOI: 10.3390/en17051129.